TRANSFER FUNCTION MODELS OF CORTICO-CORTICAL EVOKED POTENTIALS FOR THE LOCALIZATION OF SEIZURES IN MEDICALLY REFRACTORY EPILEPSY PATIENTS

by

Golnoosh Kamali

A dissertation submitted to Johns Hopkins University in conformity with the requirements for

the degree of Doctor of Philosophy

Baltimore, Maryland

October 2020

Abstract

Surgical resection of the seizure onset zone (SOZ) could potentially lead to seizure-freedom in medically refractory epilepsy (MRE) patients. However, localizing the SOZ is a time consuming, subjective process involving visual inspection of intracranial electroencephalographic (iEEG) recordings captured during invasive passive patient monitoring. Cortical stimulation is currently performed on patients undergoing invasive EEG monitoring for the main purpose of mapping functional brain networks such as language and motor networks. We hypothesized that the evoked responses from single pulse electrical stimulation (SPES) can be used to localize the SOZ as they may express the natural frequencies and connectivity of the iEEG network. We constructed patient specific transfer function models from evoked responses recorded from 22 MRE patients that underwent SPES evaluation and iEEG monitoring. We then computed the frequency and connectivity dependent "peak gain" of the system, as measured by the $\mathcal{H}_\infty$ norm from systems theory, and the corresponding "floor gain," which is the gain at which the $\mathcal{H}_\infty$ dipped 3dB below the DC gain. In cases for which clinicians had high confidence in localizing the SOZ, the highest peak gain transfer functions with the smallest "floor gains" corresponded to when the clinically annotated SOZ and early spread regions were stimulated. In more complex cases, there was a large spread of the peak gains when the clinically annotated SOZ was stimulated. Interestingly for patients who had successful surgeries, our ratio of peak-to-floor (PF) gains, agreed with clinical localization, no matter the complexity of the case. For patients with failed surgeries, the PF ratio did not match clinical annotations. Our findings suggest that transfer function gains and their

corresponding frequency responses computed from SPES evoked responses may improve SOZ localization and thus surgical outcomes.

Primary Reader and Advisor: Sridevi V. Sarma

Secondary Reader and Co-Advisor: Joon-Yi Kang

Acknowledgements

My PhD journey has been complicated and convoluted at times. To have finally reached this stage means more than I could ever properly express in words. There have been so many people throughout this process to whom I am deeply thankful and grateful for that have helped me to get to where I am today. To properly thank everyone who has been involved, I feel would require another dissertation of its own. But just know that your impact in my life is not lost on me and I would not be where I am today without you.

I would like to first and foremost thank my advisor Dr. Sri Sarma. Dr. Sarma has been an amazing advisor, role model, and someone whom I look up to. I cannot begin to express my gratitude to her for giving me the opportunity to join her lab and be a part of her amazing team. I have learned so much in my short time with her and it has ignited my passion for research and work in this field. At a time when I was struggling to believe in myself, she did and she did so with absolute confidence, no doubts or hesitations. My only regret is how short my time has been in her lab and with her. I am forever grateful for the opportunity she has provided me and the doors she has opened for me. I would like to next thank my co-advisor Dr. Joon Kang. From the moment I met Dr. Kang she has been the kindest and most supportive during my studies. I have truly enjoyed learning from her and am honored for to have been able to work with such a brilliant and hardworking neurologist. I am incredibly thankful for the amazing opportunity to work with Dr. Kang on such an exciting project that includes a rich dataset and her groundbreaking experiments.

I would like to thank my department and all the wonderful professors that I have had the pleasure of getting to know throughout my time at Hopkins. I would like especially to thank Dr. Pablo

Iglesias, whom has been supportive from the very beginning of my time at Hopkins. I would also like to thank Ms. Debra Race and Ms. Belinda Blinkoff for all their help navigating the program and for always being a friendly face I could reach out to for help.

Thank you to all my lab mates for their constant support, friendship, and valuable insights and help. I cherish all the times we have had together, and I thank you for helping to make my experience such an enjoyable one. I would like to specifically thank Kristin Gunnarsdottir for not only being such a wonderful friend, but for introducing me to Dr. Sarma, which led me on the path that I am on today. I would also like to thank Dr. Rachel Smith, the postdoctoral fellow and my dear friend whom I have been working with closely on this project. It has been a joy getting to work with you and learn from you.

I would like to thank all my friends, both near and far for their unwavering support, encouragement, and constant love. Thank you to my friends in Baltimore and Hopkins for making my time here such an enjoyable one. Thank you to my best friends from college for always keeping me sane and being with me from the beginning and thank you to everyone else in between.

I would like to thank my family both abroad in Iran and here in the States. I thank you for the endless amount of love and support you have provided me throughout my entire life and continue to do. I would like to thank my Aunt Parvin and Uncle Ahmad whom have been like a second set of parents, while I have lived here in Baltimore away from my own parents and my cousins Nada and Naseem who have been like my sisters. Thank you for providing me a home when mine at times was too far away.

Finally, I would like to like to thank my parents, my mom Behnaz, my dad Reza, and my sister, Behnoosh. There are truly no words either in English or Farsi that I could find to convey to you

how much the three of you mean to me and how thankful and lucky I feel to be a part of your lives. I know without a doubt, I would not have been able to have earned this degree if it were not for the three of you. I know this journey has been rough at times for all of us, but I thank you for sticking by me through it, for your constant, unwavering, and unconditional support, and love. Thank you to my mother for all of the sacrifices she has made my entire life and continues to do, so that Behnoosh and I may have such wonderful lives. Thank you for being the glue that binds us all together, for always believing in me, supporting me, encouraging me, loving me, and being my best friend. Thank you to my sister for always making sure I remember to enjoy life, for all the adventures we have been on, for having my best interest at heart, and for bringing so much light and joy to my life. Thank you to my father for being someone whom I could always look up to, for showing me what it means to work hard, being dedicated, and pursuing your dreams. For as long as I can remember, I have always wanted my PhD, have wanted to be like you dad, and now I can say, I will have that honor. Thank you.

Dedication

To my parents, Reza & Behnaz, and my sister, Behnoosh,
without whom none of this would have been possible.

Contents

List of Tables

List of Figures

This page intentionally left blank.

Chapter 1

Introduction & Background

1.1 What is epilepsy?

According to the World Health Organization (WHO), as many as 1 billion people worldwide suffer from neurological disorders [1]. Together with headaches, epilepsy is one of the most common chronic neurological disorders [1,2] and the fourth most common neurological illness in the United States after migraines, strokes, and Alzheimer's [1,3]. This disease plagues more than 60 million people globally, with over 150,000 people developing epilepsy each year in the United States alone [2].

Epilepsy is difficult to define because of the variable and unpredictable nature of the disease. In 2014, the International League Against Epilepsy (ILAE) updated the definition of epilepsy to be a disease of the brain that is marked by any of the following conditions: "1. at least two unprovoked (or reflex) seizures occurring more than 24 hours apart; 2. one unprovoked (or reflex) seizure and a probability of further seizures similar to the general recurrence risk (at least 60%) after two unprovoked seizures, occurring over the next 10 years; 3. diagnosis of an epilepsy syndrome" [4].

The defining characteristic of epilepsy are seizures, which are sudden recurrent episodes of abnormal electrical activity in the brain [5]. An epileptic seizure has been established as "a

transient occurrence of signs and/or symptoms due to abnormal excessive or synchronous neuronal activity in the brain" [6]. The ILAE assembled a task force in 2017 to update the classifications of seizures and epilepsies. They have classified seizures in the following categories based on their onset location: focal, generalized, and unknown or unclassifiable. Focal seizures begin in one area of the brain but can generalize and spread to other areas. Focal seizures can be further subdivided into "aware" seizures, where the patient is conscious and aware of the event, or "impaired awareness", where the patient's consciousness has been altered [5,6]. Generalized seizure onsets occur when both hemispheres of the brain are excited at the onset of the seizure, and this designation is often based on behavior and EEG. An unknown onset seizure describes a seizure whose onset is unknown, but the other manifestations of the seizure are known. Finally, unclassifiable seizures are those whose onset and manifestations are unknown [4-6].

Anti-epileptic drugs (AEDs) are first line of treatment for epilepsy. AEDs generally affect the ion channels or neurotransmitters in neurons in attempts to restore the balance of excitation and inhibition within the central nervous system (CNS) [7]. AEDs have four main goals: 1) to eliminate seizures or reduce the frequency of seizures, 2) to mitigate the adverse effects associated with long-term treatment, 3) to help patients restore or maintain their usual lifestyles, and 4) to help patients have a normal lifestyle to the highest degree possible [8].

About 30% of those with epilepsy have medically refractory epilepsy (MRE), meaning the patient's seizures cannot be managed with current AEDs [9-11]. Those with MRE are debilitated by their disease resulting in severe cognitive, physical, and emotional deficits [12-14]. This results in frequent hospitalization, making MRE patients considerable contributors (80%) to the estimated

$16 billion dollars spent annually treating epilepsy [12,13,15]. Besides the financial burden imposed, this disease inflicts great suffering on not only those with MRE by disrupting their lives, impairing their cognitive and psychological growth, and decreasing their quality of life, but also to those close to them, in terms of financial and emotional strain. This also burdens the healthcare system and society as a whole in the form of direct care costs, direct nonmedical costs, and indirect costs from lost productivity from unemployment and premature mortality [3]. With such a prevalent and life altering disease, finding a cure or effective treatment option becomes imperative.

1.2 Current treatments for MRE patients

Current treatment options for those with MRE include surgical resection/ablation or electrical stimulation of the seizure onset zone (SOZ) and early spread regions. Both options require the precise localization of the SOZ and early spread regions. In some cases, when MRE patients that have seizure onset zones (SOZ) and early spread regions that are well-defined, surgical resection or electrical stimulation may sufficiently perturb the epileptogenic network to leave the patient seizure-free. However, localization of the SOZ and early spread regions is difficult, and thus the overall seizure free rates after epilepsy surgery vary widely from 30-70% [16,17]. The lower success rates (<50%) are most often seen in patients who undergo invasive EEG monitoring prior to epilepsy surgery.

Current SOZ localization techniques fall into two areas: noninvasive passive localization and invasive passive localization. Noninvasive passive localization includes PET scans, brain MRIs, SPECTs, and scalp EEGs to locate the SOZ. These methods work well in cases when the epilepsy is caused due to a lesion or some abnormality revealed in the brain scans. However, for cases

where there are no structural lesions, these neuroimaging data do not always provide enough conclusive information to sufficiently localize the SOZ. Even high-density scalp EEG data does not have the spatial resolution to adequately localize the onset of the seizure, especially when it is believed that the seizures may originate from a deep brain structure.

When the noninvasive studies remain non-concordant or inconclusive regarding seizure localization, patients then undergo invasive EEG monitoring (see Figure 1.1). A craniotomy is performed on those patients in which they implant an electrocorticography (ECoG) grid, or the surgeons drill small holes in the skull for stereoelectroencephalography (SEEG) electrodes (both will be referred to as iEEG from now on). These patients are hospitalized for 1-2 weeks while seizure medications are slowly tapered to capture the patient's typical seizures. The iEEG recordings are then visually inspected by trained clinicians. This is often a tedious and time-consuming process, involving visual inspection of dozens of EEG signals both before and during seizures that occur over several days to weeks. To add to the complexity of visual interpretation, there is often variation in seizure onset zones when multiple seizures are captured or simultaneous onset of multiple disparate electrodes are seen. Therefore, it is not perhaps surprising that patients who undergo surgery after iEEG have the worst post-surgical seizure free rates.

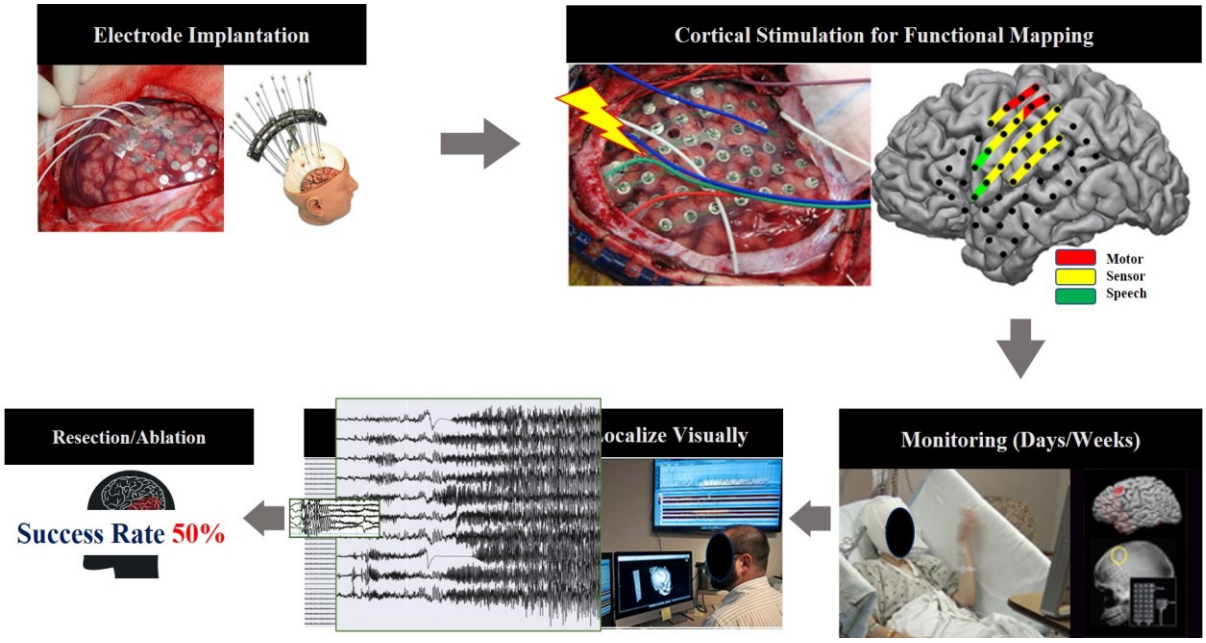

Figure 1.1 Clinical workflow for invasive passive localization. Craniotomy is performed and electrodes such as ECoG and SEEG are implanted. SPES is often undergone and cortical stimulation is used for functional mapping, after which time patients are monitored in the EMU. Clinicians visually inspect EEG signals that have been gathered during the days of monitoring and attempt to localize the SOZ. Several weeks later, clinicians perform a resection or ablation, which currently holds a 50% success rate.

1.3 Single-Pulse Electrical Stimulation

After electrode implantation, single pulse electrical stimulation (SPES) is often performed on pairs of electrode contacts for the primary purpose of mapping eloquent areas of the cortex and to determine the brain's functional connectivity. There is increasing evidence that cortico-cortical evoked potentials (CCEPs), the responses obtained from SPES, can aid in localizing the SOZ in iEEG data [18-22]. SPES evokes CCEPs [23,24]), specific waveforms whose properties can be used to define directed (effective) connections in the human brain [23,25] The neural mechanisms underlying CCEPs are still unknown [23,25] The earliest sensory response is thought to be a depolarization in the middle laminae (N1 response), followed by complex patterns of excitatory and inhibitory post-synaptic potentials to form the N2 response [25] Though the technique was first used to map inter-areal connectivity of the language [24]and motor cortices [26], the technique

has been extended to evaluate functional connections of the limbic network [27]., frontal-temporal lobe[28], the parietal-frontal lobe[29], the insula [30,31], and deeper brain structures [32,33]. Functional and pathological connectivity in epilepsy has begun to be explored with SPES to localize the epileptic networks [34].

SPES has been used as a tool to investigate cortical excitability in epilepsy as well as probing seizure networks [34]. Seizure-prone tissue may be heralded by a decreased threshold of excitability, as measured by the presence or strength of CCEPs in the stimulating or surrounding regions [34]. CCEPs have been shown to differ when stimulated or recorded in the SOZ regions as compared to in healthy tissue, and this is hypothesized to be evidence of increased excitability. For example, the amplitude of the CCEP response was found to be higher in the SOZ regions when compared to outside regions [20,35,36] as well as in early ictal propagation sites [37,38]. “Delayed responses”, a second marker of epileptogenicity, are induced by CCEPs and are identified as activities that resemble spikes or slow waves. These waveforms occur 100 ms to 1 second after the stimulation onset and have been shown to be more likely present in SOZ regions [39-41]. Additionally, it was shown that removal of areas that consistently exhibited these delayed responses resulted in good outcomes [42-44]. High frequency activity during the CCEP [45,46] may have some localizing power, as suppression of high-frequency activity after stimulation was shown to correlate with SOZ regions [47]. A standing biomarker of epileptogenic tissue, high frequency oscillations (HFOs), were found to colocalize with CCEP responses [48-50], in one study as much as 40% of the time [51]. Lastly, graph theoretical properties of the networks generated from CCEP response amplitudes revealed that networks are more bi-directionally connected in the SOZ than in non-SOZ regions [52-54].

1.4 Thesis Aims

Effective treatments and a potential cure for MRE patients is dependent upon the precise and accurate localization of the epileptogenic regions [55]. Current localization techniques involve the visual inspection of hours of iEEG data channel by channel. This visual assessment approach is not only a tedious and time-consuming process for clinicians, it also results in poor surgical success outcomes. Epilepsy, a network disease, requires analysis techniques that can capture the dynamical interactions of brain regions, unlike the current static approaches. We proposed building dynamical network models (DNMs) that can characterize the dynamics of the brain network activity and provide quantitative metrics which can be used to help clinicians precisely and objectively localize the SOZ and epileptogenic regions. Specifically, we have built patient-specific single input multioutput (SIMO) transfer function models from SPES data, analyzing several model properties to determine performance metrics that are able to reflect the epileptogenic nature of the EEG network. This methodology has been accomplished through the following aims:

Aim 1 Collecting and preprocessing SPES iEEG data: CCEPs data was gathered from 22 MRE patients treated at the Johns Hopkins Hospital who underwent SPES. The preprocessing of the data included removal of stimulation artifacts and channels deemed to be noisy and/or nonresponsive. We computed the average evoked response (ERP) from the stimulation trials for all contacts for each pair of stimulation electrodes.

Aim 2 Creating dynamical network models to reconstruct CCEPs: We constructed patient-specific single-input, multioutput (SIMO) transfer function models from CCEP recordings. First, linear time invariant state space models were estimated for the average evoked responses for all EEG channels. From these state space models, we then constructed SIMO transfer function models and demonstrated their ability to accurately reconstruct the average CCEPs for each patient dataset.

Aim 3 Correlating properties of transfer function models to the seizure onset zone: We investigated several properties of our SIMO transfer function models such as the system gain (e.g. the $\boldsymbol{\mathcal{H}}_\infty$ norm), the peak frequency at which this gain is achieved, the frequency response of the system, and the cut-off frequency at which the system's magnitude drops the fastest. We hypothesized that the electrode pairs in the SOZ and early spread regions would produce some of the largest system gains and have the biggest roll off in magnitude compared to their non-SOZ counterparts. This allowed us to define a performance metric we called the peak-to-floor (PF) ratio, which can potentially provide clinicians with a standard metric for the localization of the SOZ from SPES data.

Chapter 2

Literature Review

2.1 Current CCEP Analysis Techniques

Current computational approaches to analyzing seizure networks from CCEPs often compute iEEG features on individual channels, such as the N1 peak amplitudes and signal latencies [20-22, 56], or they compute static pairwise correlations, organize these correlations into adjacency matrices, and derive graph-theoretic measures [57,58].

CCEP responses usually consist of an early negative potential, called N1, and a late negative potential, called N2. The N1 peak occurs 10-30ms after onset of stimulation and the N2 peak occurs 80-250ms after stimulus onset [24,25]. Given the structure of CCEP responses, numerous features of the response have been studied in relation to the epileptogenic region. CCEP analysis has included the correlation between amplitude differences in CCEPs, morphological differences, and signal latencies between evoked sites and regions believed to be part of the epileptogenic network [20-22]. Several studies have shown a correlation between the N1 peak response site and stimulation site suggesting direct cortical connections. The amplitude of the N1 response has also been shown to be significantly different within the SOZ when compared to outside the SOZ [20,35-38]. It is believed then that the N1 response of CCEPs reflect the structural and functional

connections between cortical regions. Therefore, most current analysis of CCEP involves techniques evaluating the N1 response. The standard practice for determining the N1 response peak is through visual identification [20-22,56].

More recent approaches to analyzing CCEPs utilize a graph theoretic approach, investigating static metrics such as correlation across pairs of electrode responses [54,57,58]. Most often, adjacency matrices are built and different centrality measures are investigated, such as in-degree, out-degree, and katz centrality. To characterize the network topography of the epileptic brain, graph theorical analysis defines electrodes pairs and brain regions as nodes of the network with the effective CCEP amplitudes defining the edges [59-61]. Effective CCEP amplitudes are based on the weighted connectivity from the stimulating site to the recording site and considered effective if the CCEP amplitude exceeded a predefined threshold, ranging from significant z-scores to six times the standard deviation of the response [61]. The graphs are based on pair-wise interactions that aim to describe the global and local characteristics of the network. Such

2.1.1 Current Limitations

Many of these standard analysis techniques of CCEPs take an individualized channel approach either through visual inspection of the responses, or through measuring amplitude and morphological differences across responses. These approaches are limited in their ability to capture the underlying network dynamics of the disease. Computing iEEG features such as N1 peak amplitudes forgoes the network aspect of epilepsy by inspecting individual channels connection to the stimulation instead of its connections to all electrodes simultaneously. This current approach is also very time- and resource heavy, relying on hours of iEEG data to be visually interpreted by

expertly trained clinicians. This also contributes to the high levels of subjectivity in using the N1 amplitude as a metric.

While graph theoretic approaches can compute summary statistics of interest such as nodal centralities and network hubs, such measures are not based on well formulated hypotheses of the role of the SOZ in the iEEG network. Additionally, many different networks (adjacency matrices) can have identical summary statistics, providing no discriminatory power in localizing SOZ regions. The interpretations of such measures are thus ambiguous and can miss critical system properties, resulting in inaccurate and incomplete localizations of the SOZ. In contrast, dynamical network models can reveal the epileptic network connections and the underlying dynamics of seizure generation.

2.2 Dynamical Network Models

Dynamical systems are complex systems involving the interplay of time and space, whose behavior can be described with mathematical functions such as differential equations and difference equations. Dynamical network models (DNMs) are the mathematical models that describe the behavior and the connection of these complex systems. The rich theory and power of DNMs make them ideal candidates for modeling and analyzing many complex systems in our natural world, such as EEG data. The number of DNMs available are vast, from linear to nonlinear, continuous to discrete, and time domain to frequency domain. Each model provides its own advantages for different applications.

Work done by A. Li et al [77,78] showed that an epileptic brain can be modeled as a network that is on the verge of instability, where a small perturbation can result in the manifestation of a seizure.

There are nodes within this network that are potentially more "fragile" than others, corresponding to the brain regions associated with the onset of the seizure. The fragility of these network nodes makes them susceptible to small perturbations, evoking a significant response or disturbance in the network, possibly initiating a seizure. We hypothesized that these "fragile" nodes should produce large responses, responses larger than the other nodes within the network. It is also known that seizure spread is specified by impaired excitation and inhibition balance, suggesting that large responses may be a potential biomarker of this imbalance [80-83]. Therefore, we believed that the class of linear input-output models, specifically transfer functions, could best capture the dynamics of the epileptic brain network, and provide quantitative metrics which could be used by clinicians to help delineate the epileptogenic regions during localization.

2.2.1 Transfer Function Models

Transfer functions are mathematical functions that model a system's output for possible inputs. When viewed in the frequency domain, transfer functions describe a system's output as a function of the frequency of the input applied. For linear time-invariant (LTI) systems, a transfer functions can characterize the entire system by just one input, such as a step or impulse response. Though most "real" systems have non-linear input-output characteristics, when confined to certain parameters or time windows, they can exhibit LTI behavior, allowing us to use these transfer function representations [63,64].

Consider an LTI system described by the following differential equation

$$\frac{d^n y}{dt^n} + a_1 \frac{d^{n-1} y}{dt^{n-1}} + \cdots + a_n y = b_0 \frac{d^m}{dt^m} + b_1 \frac{d^{m-1} u}{dt^{m-1}} + \cdots + u \qquad (2.1)$$

where u is the input and y is the output. Taking the Laplace transform of both sides,

$$\mathcal{L}\left\{\frac{d^n y}{dt^n} + a_1 \frac{d^{n-1} y}{dt^{n-1}} + \cdots + a_n y = b_0 \frac{d^m}{dt^m} + b_1 \frac{d^{m-1} u}{dt^{m-1}} + \cdots + b_m u\right\} \quad (2.2)$$

we end up with

$$s^n + a_1 s^{n-1} + \cdots + a_n = b_0 s^m + b_1 s^{m-1} + \cdots b + u \quad (2.3)$$

The differential equation can be completely described by the following two polynomials

$$a(s) = s^n + a_1 s^{n-1} + \cdots a_{n-1} s + a_n$$
$$b(s) = b_0 s^m + b_1 s^{m-1} + \cdots b_{m-1} s + b_m \quad (2.4)$$

where *a(s)* is the characteristic polynomial of the system [60, 61].

The transfer function is then the rational function

$$H(s) = \frac{b(s)}{a(s)} \quad (2.5)$$

where the polynomials *a(s)* and *b(s)* are given by (2.4). The above describes a single-input, single-output (SISO) transfer function. This same idea can be generalized to multi-input, multi-output (MIMO) systems, which is a matrix of rational functions that relates the outputs to the inputs, and single-input, multi-output (SIMO) systems, which is a vector of rational functions, relating the outputs to one input [62,63].

2.2.1.1 Properties

One of the many advantages of using transfer functions is the rich theory, literature, and properties that come with it given their importance in linear systems and control theory. As mentioned earlier, transfer functions can characterize a system's output as a function of the frequency of the input

applied. Formally, this can be defined as evaluating the transfer function *H(s)* in (2.5) at the complex frequency $j\omega$,

$$H(s)|_{s=j\omega} = H(j\omega) = |H(j\omega)|e^{<H(j\omega)} \quad (2.6)$$

We refer to (2.6) as the frequency response of the system, where $|H(j\omega)|$ is the amplitude

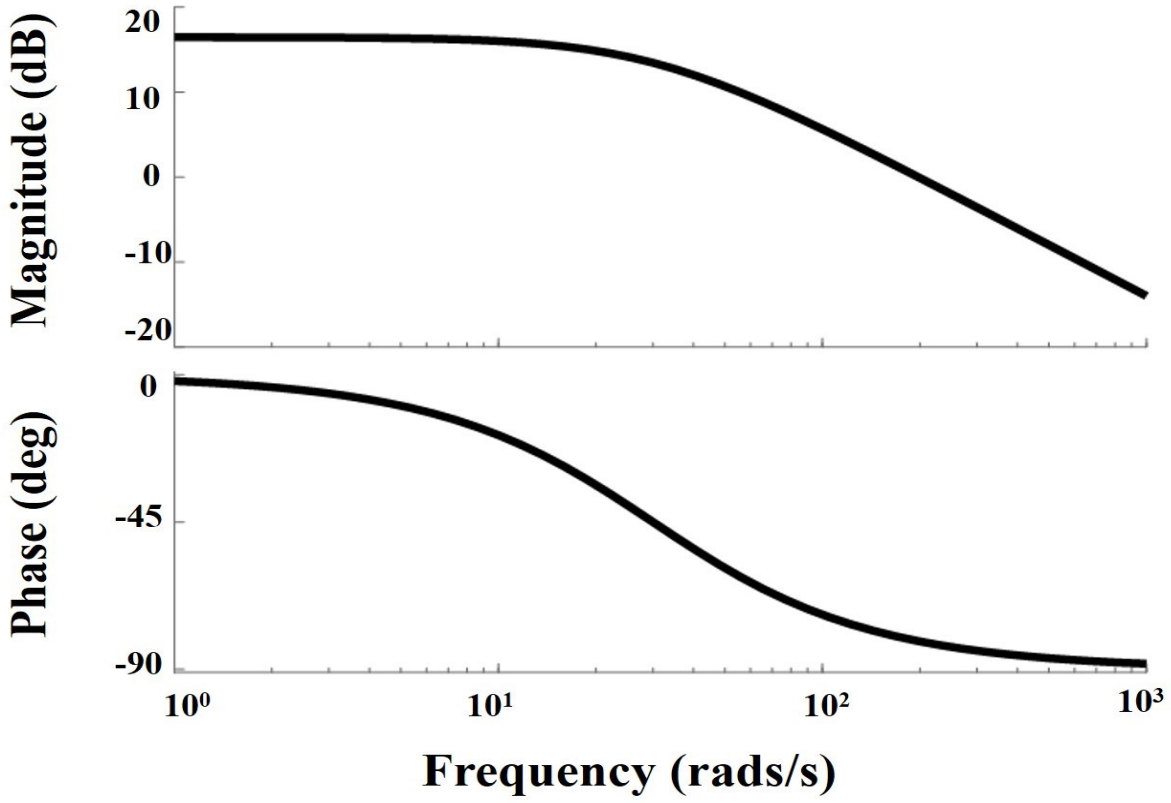

Figure 2.1. Bode plot example of SISO system. Top plot is the magnitude of the system plotted over all frequencies and bottom plot is the phase of the system plotted over all frequencies

response, $< H(j\omega)$ is the phase response, ω is the frequency, and j denotes the imaginary number [62,63]. The frequency response can be visualized through a bode plot, which plots the magnitude of the frequency response over the range of frequencies, ω (Figure 2.1).

From the frequency response we can determine things such as the peak magnitude or maximum response of the system at a particular frequency, the smallest response at a particular frequency, and how quickly the system drops off in magnitude.

Chapter 3

Methods

3.1 Experimental Protocol with SPES

3.1.1 Patients

Our patient database consisted of retrospective datasets of 22 MRE patients who underwent iEEG monitoring and SPES for the localization of seizures at Johns Hopkins Hospital (JHH) Epilepsy Monitoring Unit (EMU). Patient consent had been obtained as part of the Studies of Patients with Implanted Electrodes (IRB 000444461). Patients underwent invasive-passive monitoring for an average of 8 days, while medications were tapered off for the observation of seizures. At least two board certified epileptologists reviewed the patient iEEG data, identifying electrodes involved in regions of seizure onset (SOZ), early spread (EP), and irritative (IZ) zones. Seizure onset was defined as the first consistent presence of rhythmic spikes, rhythmic sharp waves, regular or low amplitude activity in the beta range, or recruiting gamma activity that was either prior or coinciding with the clinical manifestation of the seizure. The early spread regions were defined as those areas to which the seizure activity spread before secondary generalization occurred [65].

Patients were classified as having successful surgical outcomes if they experienced seizure freedom one-year after surgery (Engel class 1) and a failed outcome if they have seizure recurrence (Engel classes 2-4)[63] (Table 1, Supplementary). Thirteen of the 22 patient have had surgery and evaluated for surgical outcome. Due to the lack of outcome data in the remaining nine patients, we

categorized all patients by a custom "clinical complexity (CC)" score (Figure 3.1) [56,67]. These categories were developed in light of previous outcome studies that showed that patients with visible lesions on MRI (lesional) have higher surgical success rates (approximately 70%), while non-lesional, extratemporal, and multifocal epilepsies have much lower success rates [68-70] (Figure 3.1). Table 1 summarizes the main clinical information for all patients, including pathology, seizure type, and MRI SOZ onset.

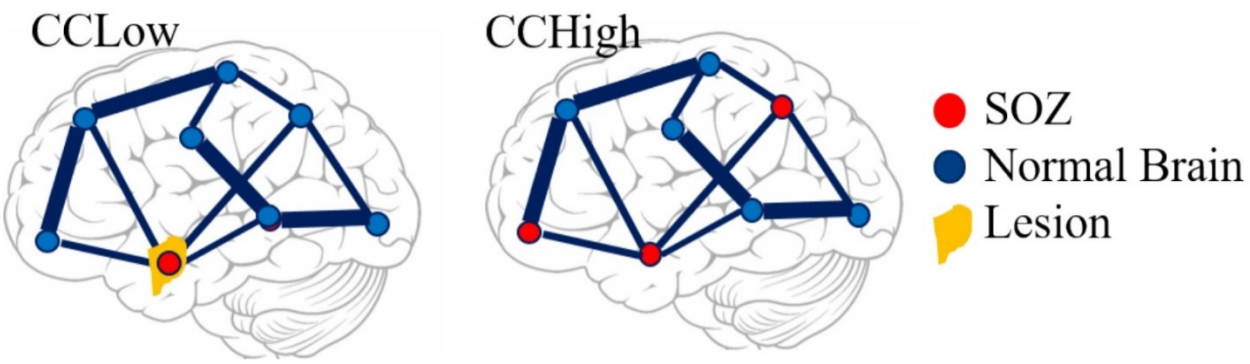

Figure 3.1 Pictorial representation of clinical complexity. CCLow was defined as cases that were lesional, only one seizure focus, or solely confined to the temporal lobe. CCHigh was defined as cases of multi-focal epilepsy, a seizure focus outside the temporal lobe, and/or no lesions on imaging.

3.1.2 Single-Pulse Electrical Stimulation

SPES was conducted in a bipolar fashion on adjacent electrode pairs in the clinically annotated the SOZ and early spread regions as well some outside of the SOZ. A monophasic, alternating polarity, 0.3ms width square wave pulse at a fixed frequency of 0.5Hz was delivered to all the electrode pairs an average of 50 times using a Blackrock acquisition system at a sampling rate of 1KHz and at times 2KHz [71]. Current intensity was titrated until there were manifestations of local/distant evoked response potentials (ERPs), discharges/seizures, or a maximum intensity of 12mA was reached. A 5mA stimulus intensity was most often used. Responses were recorded from all

channels during the 50 trials. The data was digitized and stored in an IRB-approved database compliant with the Health Insurance Portability and Accountability Act regulations. Data was then preprocessed as .dat files for analysis in MatLab [72]. The research protocol was approved by the Institutional Review Board and informed consent was obtained from all participants.

3.2 Building LTI Models

3.2.1 iEEG Preprocessing

Stereotyped responses were captured from all channels during the 50 trials. From these responses the average evoked CCEP was computed for every contact in 2 second epochs. We included 500ms of data before stimulus onset and 1500ms post stimulus onset. We calculated the distribution of the 50 time series responses for each 2 second window and marked channels as artifactual if the

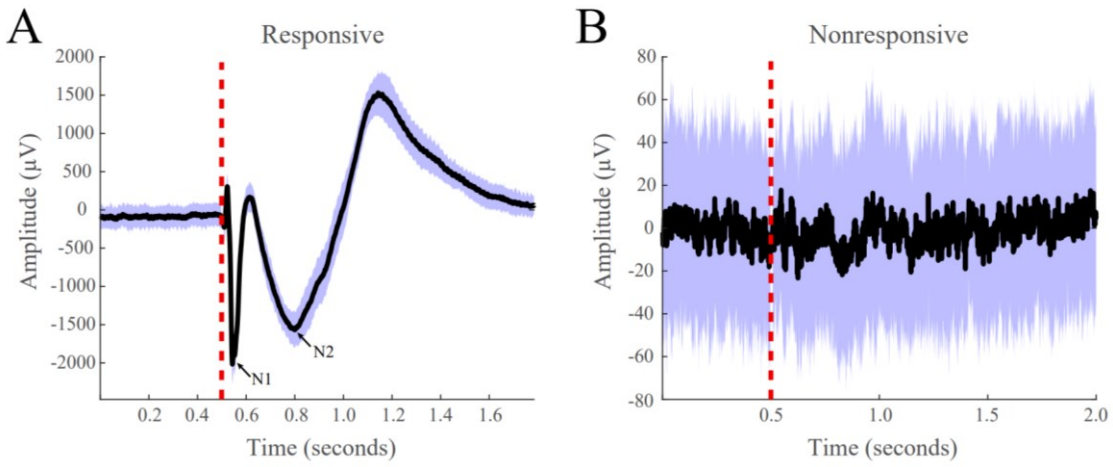

*Figure 3.2: Examples of responsive and nonresponsive waveforms from patient iEEG data. (**A**) Responsive CCEPs were defined as an absolute value of the post-stimulus amplitude greater than 100 μV from the baseline. The N1 and N2 peak are labeled. (**B**) Nonresponsive CCEP that does not meet the 100 μV post-stimulus amplitude threshold. The black line indicates the average evoked response, the purple boundaries denote one standard deviation, and the red vertical dotted line indicates the stimulation onset.*

median standard deviation of the sample distributions was greater than 1000 μV. Artifactual

channels were then zeroed out in the dataset. Next, artifacts due to electrical stimulation were removed by linearly interpolating the data 2ms before and 8ms after stimulus onset.

We classified channels as responsive and non-responsive if the absolute value of the maximum post-stimulus amplitude was greater than $100\mu V$ (Figure 3.2). Non-responsive channels were removed from the dataset before model construction [73,74].

3.2.2 LTI State Space Model Construction

Stable, discrete linear time invariant (LTI) state space models were constructed of the following form for each stimulating contact pair:

$$\boldsymbol{x}(t+1) = \boldsymbol{A}\boldsymbol{x}(t) + \boldsymbol{B}u(t) \qquad (3.1)$$

where $\boldsymbol{x}(t) \in \mathbb{R}^{N\times 1}$ is the state vector, $\boldsymbol{A} \in \mathbb{R}^{N\times N}$ is the state transition matrix, $u(t) \in \mathbb{R}$ is the input stimulation pulse, and $\boldsymbol{B} \in \mathbb{R}^{N\times 1}$ is the input matrix, with N representing the total number of contacts for each dataset. $\boldsymbol{A}$ and $\boldsymbol{B}$ were calculated via least-squares estimation as described in [75], where the state vector was comprised of the responsive iEEG signals (Figure 3.3). The models were stimulated with input signal $u(t)$ = 0 or 1, where the first nonzero element corresponded to the iEEG stimulation onset, with a pulse duration of two milliseconds. The stimulation pair electrodes were not included in the models as state variables and were instead characterized as providing the exogenous input $u(t)$ [73,74]. Next, to improve our model fits, we established a scaling factor, α, based on the range of data $\boldsymbol{x}(\boldsymbol{t})$ in relation to the range of the model reconstruction $\widehat{\boldsymbol{x}}(\boldsymbol{t})$ for every contact, *k*:

$$\alpha_k = \frac{\max x_k(t) - \min x_k(t)}{\max \widehat{x_k}(t) - \min \widehat{x_k}(t)} \qquad (3.2)$$

We then scaled our $\boldsymbol{A}$ and $\boldsymbol{B}$ by this factor, giving us the following:

$$\overline{\boldsymbol{x}}(t+1) = \overline{\boldsymbol{A}}\boldsymbol{x}(t) + \overline{\boldsymbol{B}}\boldsymbol{u}(t) \qquad (3.3)$$

where $\overline{\boldsymbol{A}} = \alpha \boldsymbol{A}$ and $\overline{\boldsymbol{B}} = \alpha \boldsymbol{B}$. One thing to note is that though the above state space model equation is written in continuous time, for implementation purposes, our models were in discrete time with an average sampling rate of 1kHz.

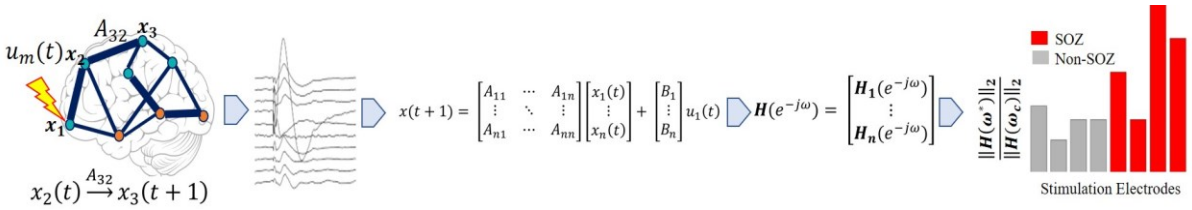

Figure 3.3: Pipeline to obtain ratio from system gain H_∞ to cut-off gain from individual patients' SPES iEEG data. Starting from top left, a brain region is stimulated. Then a stereotyped response is extracted for each electrode, from which the average evoked CCEP is calculated. The CCEPs are used to construct a state-space model. From the state space model, a SIMO transfer function vector is constructed via $\boldsymbol{H}(z) = \boldsymbol{C}(zI - \boldsymbol{A})^{-1}\boldsymbol{B}$. Then the system gain is calculated for every stimulation pair through $\|\boldsymbol{H}\|_\infty = \sup_{\omega \epsilon \mathbb{R}} \sigma_{max}\left(\boldsymbol{H}(j\omega)\right)$ and the maximum system gain and its associated frequency response is computed resulting in the network response system ratio. The expectation is that the true SOZ contacts will have the largest system gain ratio.

3.2.3 Transfer Function Model Construction

Multivariate transfer functions were constructed for each stimulating electrode pair within each subject to estimate the behavior of the CCEPs. To construct our transfer function models we then calculated single-input, multi-output (SIMO) transfer function models for each stimulation pair and contact $u(t)$ to $\boldsymbol{x}(t)$ via the formula

$$\boldsymbol{H}(z) = (zI - \overline{\boldsymbol{A}})^{-1}\overline{\boldsymbol{B}} \qquad (3.4)$$

which is derived by taking the z-transform of (3.3). These transfer function models represent the input-output behavior of CCEPs under SPES.

3.3 Investigating Model Properties

3.3.1 System Gain

We investigated whether properties of SIMO transfer function models correlated to the clinically annotated epileptogenic network. We first explored the system gain. Consistent with the theory of "fragility" in epileptic brain networks, [77,78], we hypothesized that perturbing unstable nodes in the network, i.e. epileptogenic regions, should produce the largest network responses and result in the largest system gains, quantified by the $\mathcal{H}_\infty$ norm.

We computed the $\mathcal{H}_\infty$ norm of every stimulation electrode pair i, as follows:

$$\|\boldsymbol{H_i}\|_\infty = \sup_{\omega \epsilon \mathbb{R}} \sigma_{\max}\left(\boldsymbol{H_i}\left(e^{-j\omega}\right)\right) \qquad (3.5)$$

where $\sup_{\omega \epsilon \mathbb{R}}$ denotes the supremum or least upper bound over all real frequencies ω and σ_{max} denotes the maximum singular value of the vector $\boldsymbol{H_i}$.We hypothesized that those electrode pairs with the highest $\boldsymbol{\mathcal{H}}_\infty$ norm would correspond to the electrode pairs in the clinically annotated SOZ, particularly for patients of low clinical complexity [76].

3.3.2 Cutoff Frequency

Though preliminary results showed correlations between large system gains and epileptogenic regions, other properties associated with the system gain still needed to be explored, to potentially provide multiple features that can delineate the SOZ and early spread regions. Other parameters examined were the frequency at which the maximal gain was achieved and the cut-off frequency at which the magnitude response began to drop off rapidly. For every system gain we calculated

there was a frequency ω^* at which this maximum gain was achieved, $\left\|\boldsymbol{H_i}\left(e^{-j\omega^*}\right)\right\|_\infty$. Similarly, there is a frequency at which the magnitude of the frequency response begins to drop off, known as the cutoff frequency, ω_c. The cutoff frequency denotes the boundary of where the energy flowing through the system begins to reduce. To determine ω_c, we first calculated the DC gain, which is the magnitude of the system at steady-state, i.e. $\left\|\boldsymbol{H_i}(e^{-i0})\right\|_2 = \|\boldsymbol{H_i}(1)\|_2$. Then we determined the frequency at which the magnitude response is 3dB below the DC gain. The 3dB drop is a fundamental concept in circuit theory and known as the "half-power point" [76]. At the half-power point the frequency response drops from its maximum output and continues to do so at a fixed rate [76]. We conjectured that around this value is when the system has the fastest decline. We then computed the magnitude of the frequency response of the system at this cutoff frequency ω_c, which gave us the magnitude at which the system begins to drop off

$$\left\|\boldsymbol{H_i}(e^{-j\omega_c})\right\|_2 = (\sum|h_i|^2)^{\frac{1}{2}} \qquad (3.6)$$

We conjectured that these large system gains, which are in response to small perturbations, would be associated with a fast roll off in magnitude, which could be captured by a small response at the cutoff frequency, implying that electrode pairs in the clinically annotated SOZ would have some of the smallest drop off norms when compared to non-SOZ regions [76].

3.3.3 Peak-to-Floor Gain Ratio

Given these two parameters of system gain and its associated input direction, we proposed a performance metric which can capture the large system responses and its coupled input norm through a ratio of the system gain to the input norm. We hypothesized that epileptogenic regions

when stimulated should result in a high ratio of gain to input norm. We have called this metric the peak-to-floor (PF) gain ratio, and it is defined as follows:

$$PF_i = \frac{\|\boldsymbol{H_i}(\omega^*)\|_2}{\|\boldsymbol{H_i}(\omega_c)\|_2} \qquad (3.7)$$

where i represents every stimulation electrode pair, ω^* is the peak frequency at which the maximum system gain was attained, and ω_c is the cutoff frequency at which the 3dB drop in magnitude occurred (Figure 3.4) [72].

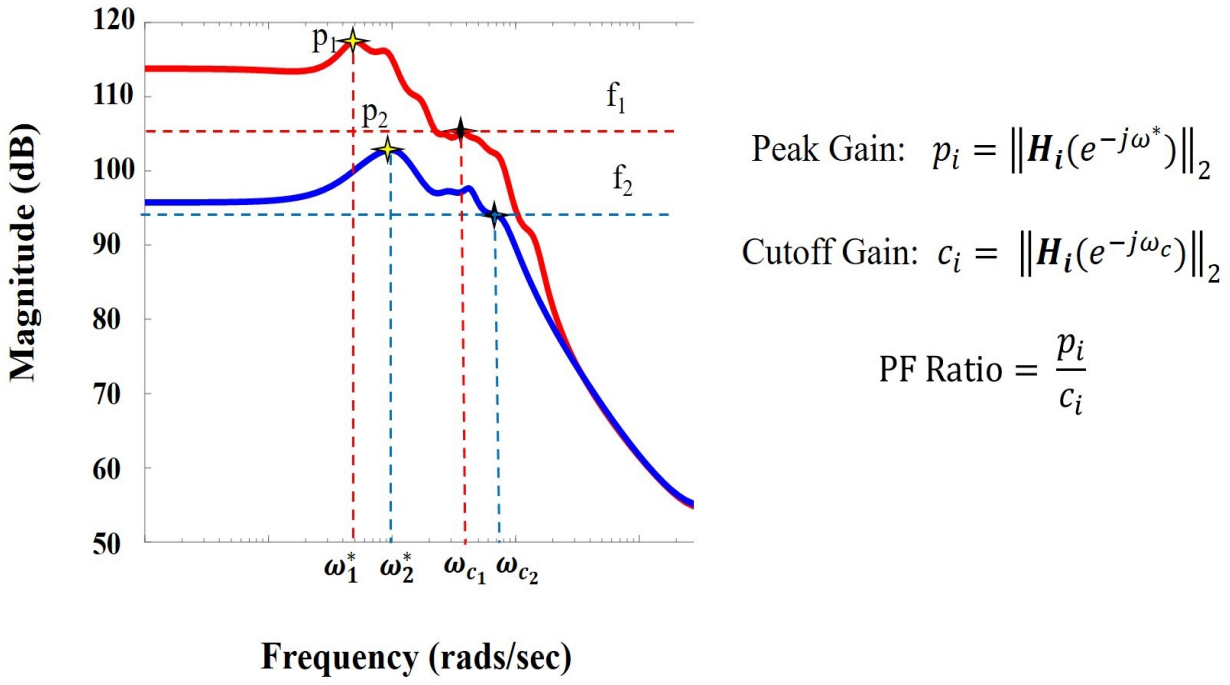

Figure 3.4 Pictorial representation of the PF ratio and its calculation. Representative bode plot of two transfer function models, where red denotes a clinically annotated SOZ dataset and blue denotes a dataset stimulated that is not part of the epileptogenic region, with their labeled peak and cutoff frequencies, ω^* and ω_c, respectively. The floor/cutoff frequency is defined as the frequency for which the magnitude is 3dB less than the gain at frequency 0, $\omega = 0$ (DC gain).

3.4 Correlating PF Ratio to Epileptogenic Regions

Once the PF ratio was computed, we measured the agreement between our models and the clinical annotations through a confidence statistic (CS). We defined the CS to be the ratio of the mean of the PF ratio of those stimulation pairs in the clinically annotated SOZ and EP to the mean of the PF ratio of all other stimulation pairs

$$CS = \frac{\frac{1}{m}\sum_{SOZ\&EP} PF_i}{\frac{1}{n-m}\sum_{Other} PF_i} \qquad (3.8)$$

where m is the number of stimulation pairs in the SOZ and EP regions, n is the total number of stimulation pairs, and *other* is all the stimulation pairs not in the SOZ or EP. We expected the highest system ratios of patients with a lower clinical complexity score (CCLow) to closely match the clinical annotations, resulting in a higher confidence statistic. On the other hand, patients with a higher clinical complexity score (CCHigh) may show more disagreement between the model results and the clinical notations, resulting in a lower and more variable confidence statistic.

3.5 Correlating CCEPs Amplitude to Epileptogenic Regions

In the current SPES literature, there are numerous methods for CCEP analysis. The most common practice is visual inspection of the peak response amplitude, more precisely, the N1 response (Figure 3.2A). The N1 responses are early sharp negative responses occurring anywhere from 10-30ms post stimulation and are believed to reflect the direct structural connections (Figure 3.2) [25]. For our study, to be able to compare the N1 response with our system ratio, we calculated the N1 peak for all evoked potentials. This was done after the preprocessing of our data in which we looked at a window 10 ms to 30 ms after the onset of stimulation. Within that time frame, the

maximum absolute peak amplitude was calculated, which we called the N1 peak, for all output contacts. We then calculated our confidence statistic using the N1 peak.

Chapter 4

Results

4.1 Transfer Function Models Reconstruct CCEPs

We first assessed whether the SIMO transfer function models were able to accurately reconstruct CCEPs by calculating the percentage of data points that lied within the 95% confidence interval of the mean from the 50 stimulation trials. This resulted in an average concordance of 92.96%

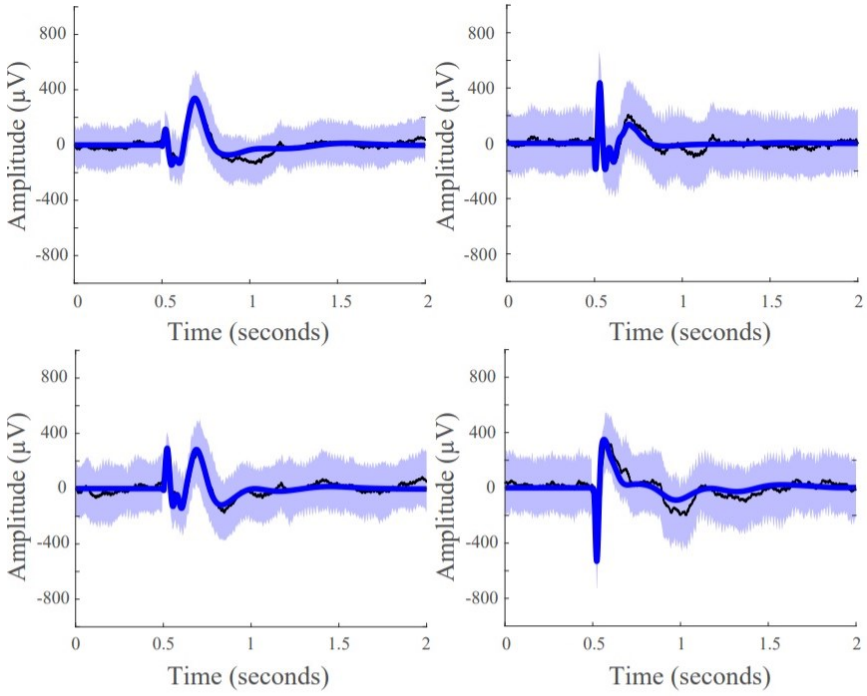

Figure 4.1: Model fits of 4 representative responsive channels from patient data showing SIMO transfer function models capture CCEP responses in recording electrodes. Black lines are the average the evoked responses, blue lines are the model reconstruction, and the purple boundaries denotes one standard deviation.

indicating that our models were able to accurately reconstruct the mean waveforms of our data, capturing the input-output behavior of CCEPs under SPES (Figure 4.1).

4.2 Higher System PF Ratios in the Seizure Onset Zone for Low Clinical Complexity Cases

In cases of low clinical complexity, our expectation was that our models would agree with the clinical annotations, and in cases of high clinical complexity there would be high variability of agreement between our model statistics and clinical annotations. We further hypothesized that successful surgical outcomes would show high agreement regardless of clinical complexity.

Patient 13 is an example of a low clinical complexity case (CCLow) and Patient 14 is an example of a high clinical complexity case (CCHigh) (Figure 4.2). These two cases showed alignment with our hypothesis in the low clinical complexity cases, our PF ratios were the highest in the areas of the clinical annotated SOZ as well as early spread regions resulting in a higher confidence statistic, while in the higher complexity case, the highest PF ratios were not in areas deemed to be part of the epileptogenic network.

In Patient 13, the largest ratios were associated with stimulation pairs that were in the SOZ (Figure 4.2A). Further, most other contact pairs in the EP and IZ (orange and yellow, respectively) also yielded high ratios, while the two electrodes pairs believed to not be part of the epileptic network (grey) had the smallest ratios. The high degree of agreement between our model gains and the clinical annotations resulted in a CS of 1.0349.

In Patient 14, the largest PF ratios were in areas outside of the clinical annotations (Figure 4.2B), where the average PF ratio of 27.550 for the SOZ and EP electrodes and an average PF ratio of 80.2357 in all other electrode pairs.

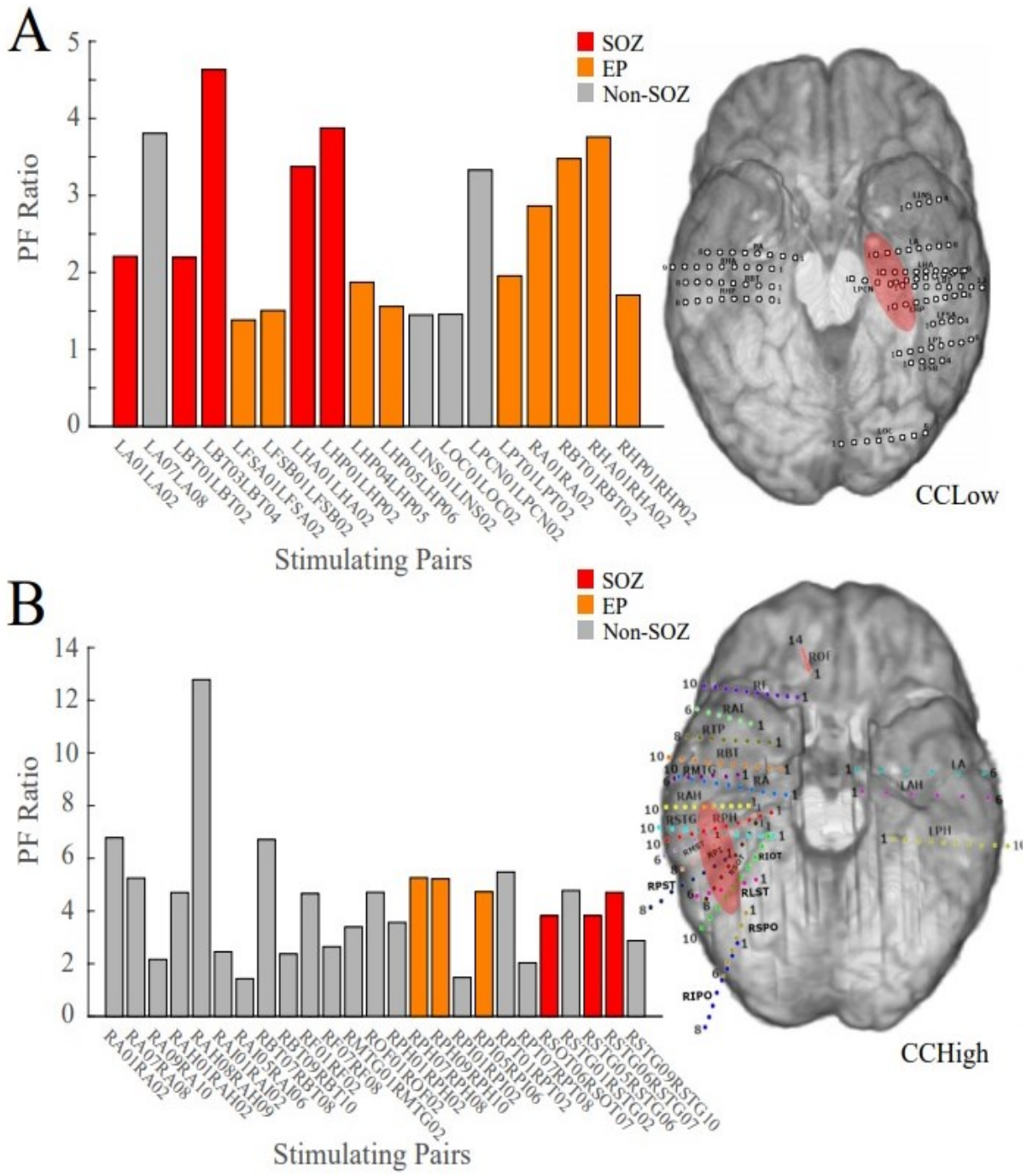

Figure 4.2 Bar plot of the peak-to-floor gain ratio, where red indicates electrode pairs in the clinically annotated seizure onset zone (SOZ), orange indicates early spread (EP), and grey represents all others. To the right of the bar graphs are the electrode implantation maps for each patient with the clinical annotated SOZ denoted in red. (A) PF ratio of representative "model success" Patient 13 dataset; high system ratio values closely correspond with SOZ and EP regions. (B) PF ratios of representative "model disagreement" Patient 14A dataset; SOZ and EP system ratios are indistinguishable from non-epileptogenic regions.

4.3 Faster Magnitude Roll-Offs in Successful Patient Outcomes

In successful surgical outcomes, where clinicians were able to accurately localize the SOZ, we anticipated frequency response plots similar to the ones in Figure 3.4, where the SOZ stimulated dataset would have a high peak gain and a quick roll-off in magnitude compared to the non-SOZ stimulated datasets. The mean frequency response plot of the SOZ and EP stimulated datasets of Patient 18, a surgical success, had a high peak gain and a big roll-off compared to the non-EZ stimulated datasets (Figure 4.3A). In the failed surgical outcome case of Patient 3 (Figure 4.3B), the SOZ stimulated dataset not only had a very small peak gain, but a rather slow roll-off as well. However, the non-SOZ stimulated datasets had overall the highest peak gains and incredibly fast roll-offs, suggesting that these datasets may be part of the epileptogenic region.

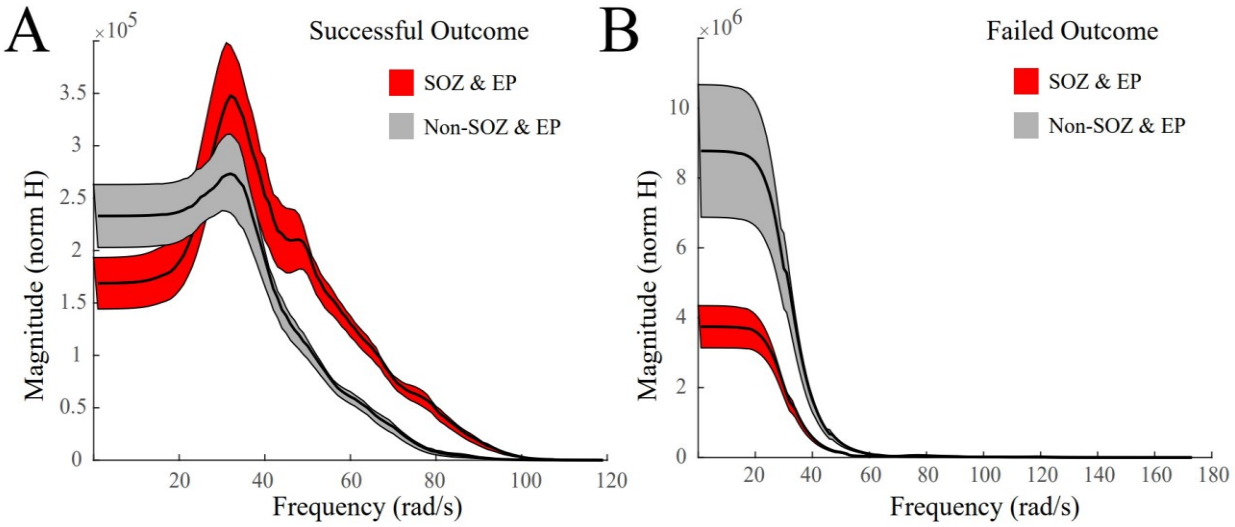

Figure 4.3 Representative frequency response plots of a successful and failed surgical outcome where red denotes epileptogenic zone (EZ) stimulated datasets, grey denotes non-EZ stimulated datasets, black is the mean frequency response, and the shaded regions denote ± 2 standard error. (A) Frequency response plot of the EZ stimulated datasets vs the non-EZ stimulated datasets for successful surgical outcome Patient 18. The EZ stimulated datasets show a larger peak gain and a bigger roll off than the non-EZ counterparts. (B) Frequency response plot of the EZ stimulated datasets vs the non-EZ stimulated datasets for failed surgical outcome Patient 3.

4.4 Correlating Surgical Outcomes to PF Ratios

We have summarized our findings for all 22 patients with three different scatter plots (Figure 4.4). The first plot displays the confidence statistic for all patients classified in terms of their clinical complexity, confidence statistic, and surgical outcome if available (Figure 4.4A). The second plot displays the confidence statistic for only those patients with surgical outcome classified in terms of their confidence statistic and either surgical failure or success (Figure 4.4C). Finally, the last scatter plot again displays the confidence statistic for patients with surgical outcome but has now separated outcomes in terms of the Engel Score (Figure 4.4E). The dotted line indicates the degree of agreement boundary, where CS values above the line indicate patients whose highest PF ratios agreed most with the clinically annotated SOZ and EP regions, and thereby implying a greater chance of surgical success, while those CS values below the line indicate patients whose highest PF ratios varied most with clinical annotations, and potentially imply a greater chance of surgical failure. This degree of agreement boundary was chosen as such based on our hypothesis that higher PF ratios would be in the SOZ and EP stimulated compared to those contacts not in the epileptogenic regions. Therefore, if clinicians were able to localize the SOZ and EP regions, then we would expect to have high PF ratios in these contacts resulting in a confidence statistic that was greater than one. However, if clinical annotations were not correct, then we would anticipate our model would have low PF ratios in those regions and higher PF ratios in other regions that the clinicians were unable to localize visually resulting in a confidence statistic less than one.

We tested whether the transfer function models were able to not only localize the SOZ, but also anticipate the surgical outcome for seizure freedom. Overall, in the MRE patients who underwent resective surgery and had a successful outcome (ES I and ES II), indicating the clinicians were

able to successfully localize the SOZ, our models had the highest PF ratios in the clinically annotated SOZ and therefore a high confidence statistic (CS > 1), irrespective of the clinical complexity (Figure 4.4A). In the surgical resection cases that resulted in poor seizure outcomes (ES III and ES IV), suggesting the clinicians were unable to precisely and accurately localize the SOZ, our models exhibited low PF ratios in the clinically annotated SOZ and larger PF ratio values in areas that were not part of the clinically annotated SOZ (CS < 1) (Figure 4.4A). Thus, we conjecture that in patients that have undergone surgical resection/ablation, a high concordance between our models and clinical annotations would suggest seizure freedom, while large variations between our models and annotations would suggest a poor surgical outcome.

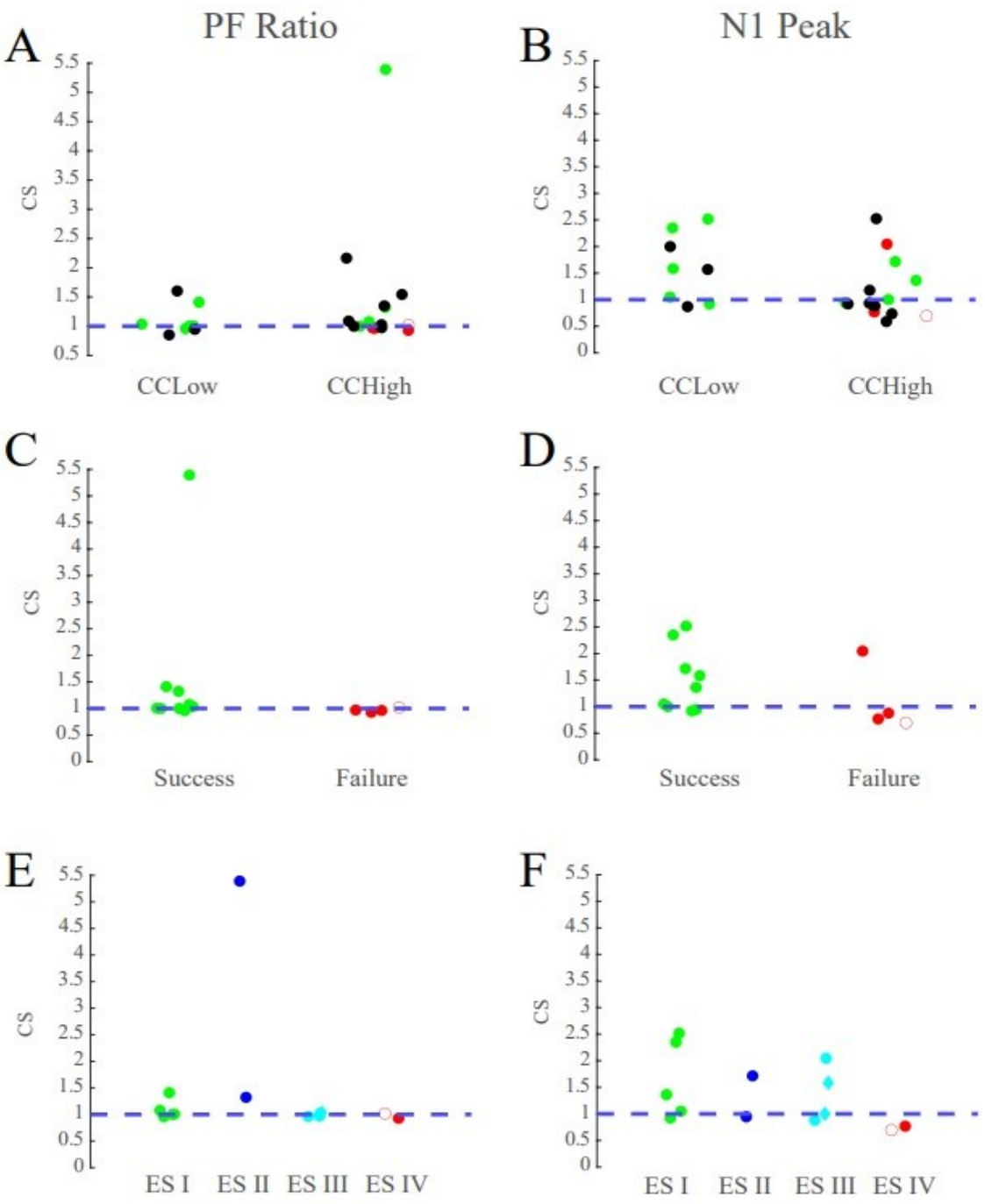

Figure 4.4 Peak-to-floor gain ratio confidence statistic reflects surgical outcome. Green circles denote those patients with successful surgical outcomes, red denotes those with failed surgical outcomes, and black denotes datasets that currently have no surgical outcome. The blue dotted line denotes the boundary for the degree of agreement between clinical annotations and the performance metrics. Diamond shape indicates RNS patients and open circle indicates outlier Patient 5. (A) The confidence statistic plot for PF ratio. CCLow patients often have CS>1, and surgical success nearly always have CS values greater than 1. (B) The confidence statistic plot for N1 peak. Less distinction is provided between groups according to the N1 amplitude as compared to system gain. (C,D) Confidence statistic plot for surgical patients categorized by surgical outcomes for (C) PF ratio (D) and N1 peak. (E,F) Confidence statistic plot for surgical patients categorized by Engel score for (E) PF ratio and (F) N1 peak.

4.5 Cross-Validation

To test how robust our confidence statistic was in predicting surgical outcomes, we did a cross-validation test. Given our limited surgical outcome sample size of 13, we performed a leave-one-out cross validation scheme. We systematically removed one patient each iteration and fit a logistic regression model on the remaining 12 patients. Specifically, for $p_i = Prob(success\ for\ patient\ i)$, we built the following model:

$$log\left(\frac{p_i}{1-p_i}\right) = \beta_0 + \beta_1(CS_i) \qquad i = 1,2,\dots,13. \quad (4.1)$$

From the model, we computed an ROC by classifying the patients in the training set at various thresholds. We found the optimal threshold for each partition and applied this threshold to the test patient left out. Specifically, we determined the $\hat{p}$ for each patient that was left out, computed the outcome, and added it to the confusion matrix, resulting in the final confusion matrix shown in Figure 4.5C. From the final confusion matrix accuracy = 0.6923, sensitivity = 0, and specificity = 0.6923 and with a mean AUC of 0.8056 ± 0.0480 (Figure 4.5).

Standard practice when assessing computational algorithms for the localization of the SOZ is to use clinical annotations of the epileptogenic regions. However, in an effort to investigate the ability to build a blind biomarker metric, we assessed the correlation between features of the PF ratio and clinical complexity of patients. Specifically, for each dataset, we looked at the following features: mean PF ratio, variance of the PF ratio, the maximum PF ratio over the minimum PF ratio, and a combination of any of the two. For this validation scheme we now used all 22 patients as our observations, which allowed us to use a 5-fold validation test, with a 20% test and 80% training set. We partitioned our dataset into 5 test and validation sets, where for each test set we left out 4 patients, making sure the same patient was not left out

multiple times. We then fit a logistic regression model as defined above in equation 4.1 to our training sets, determined the outcomes for the validation sets and populated a confusion matrix. We found that the combination of the features of mean PF ratio and the max PF ratio/min PF ratios, which resulted in a mean AUC of 0.6071 ± 0.807 and the feature of PF variance, which had a mean AUC of 0.6381 ± 0.450 may potentially correlate with the clinical complexity of a patient. This could then possibly predict surgical outcomes without knowledge of clinical annotations a priori (Figure 4.6 and Figure 4.7). For the two features of mean PF ratio and max PF ratio/min PF ratio, we found an accuracy = 0.25, sensitivity= 0.25, and specificity = 0. For the feature of the variance of PF we found accuracy = 0.30, sensitivity = 0.2632, and specificity = 1.0.

However, the caveat is that in both cross-validation schemes, the limitation lies in that not every implanted contact was stimulated during SPES. A subset of the implanted electrodes, chosen by the clinical team, were stimulated, and this subset may have included any combination of clinically annotated SOZ contacts, EP, and potentially some outside the epileptogenic region. We also recognize that clinical complexity is not a definitive measure of surgical outcome, as can be seen in even in our small cohort that though a patient may be of high clinical complexity, the clinical localization may be correct, resulting in surgical success. These all indicate the very many nuances and difficulties involved in the localization of the SOZ as well as in the ability to create and assess computational metrics used in localization.

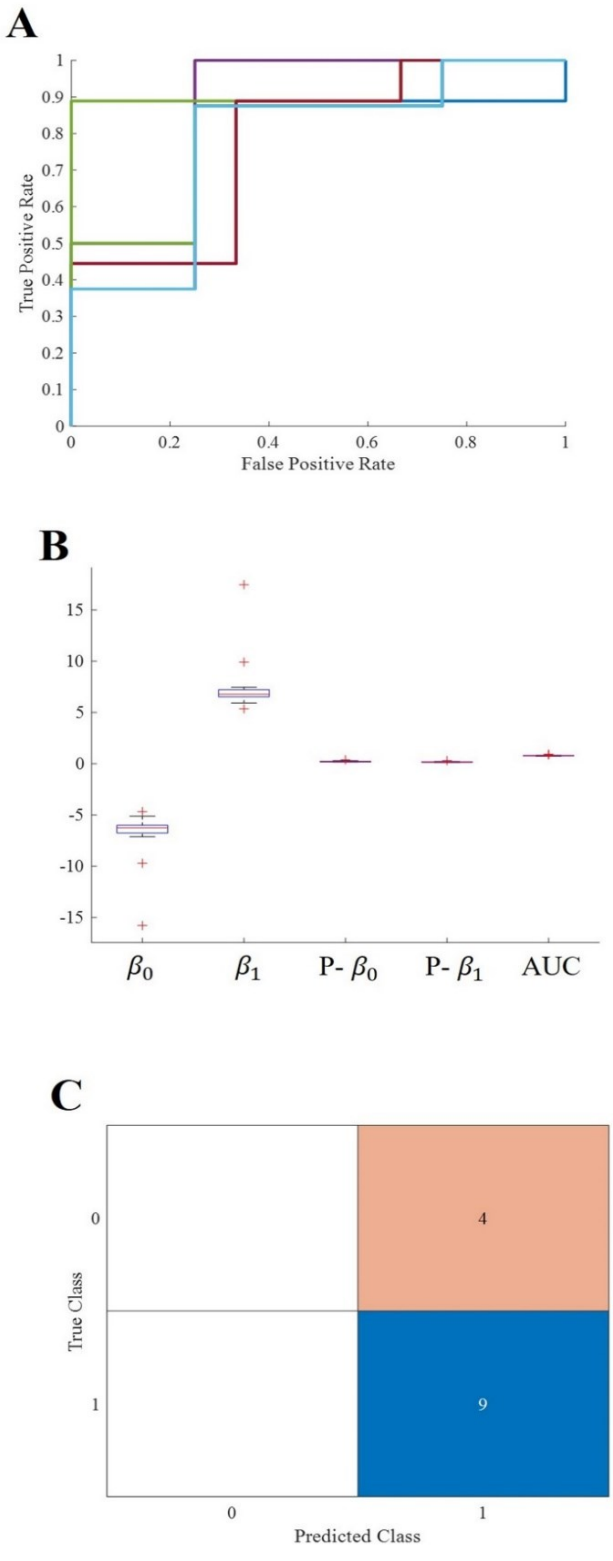

Figure 4.5 1-fold cross validation for surgical outcomes with feature of confidence statistic. (A) ROC curves overlaid from all logistic regression models in the 1-fold validation scheme. Mean AUC was 0.8056. (B) Box plots of model statistics, including beta coefficients, p-values, and AUCs. (C) Final populated confusion from validation scheme, indicating an accuracy of 69.23%.

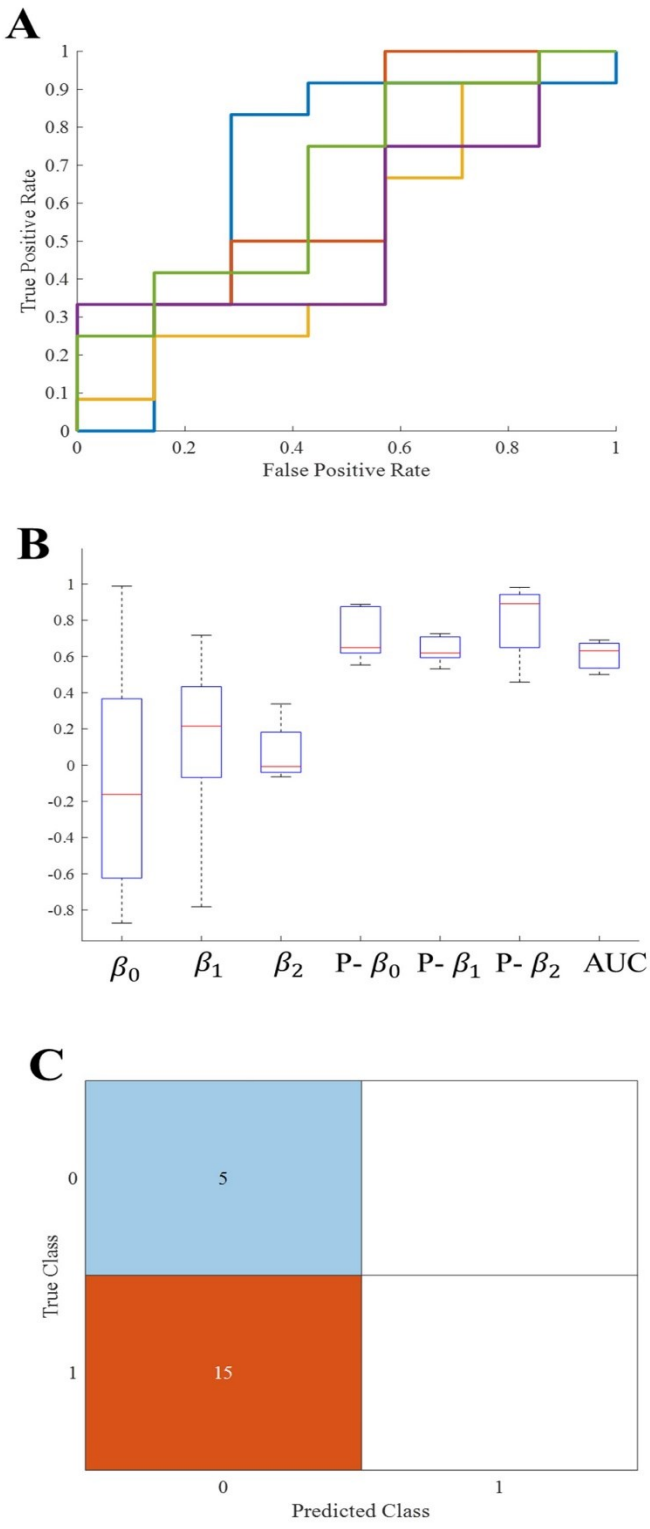

Figure 4.6 5-fold cross validation for clinical complexity with the features of mean PF ratio and max PF ratio/min PF ratio. (A) ROC curves overlaid from all logistic regression models in the 5-fold validation scheme. Mean AUC was 0.6071. (B) Box plots of model statistics, including beta coefficients, p-values, and AUCs. (C) Final populated confusion from validation scheme, indicating an accuracy of 25%.

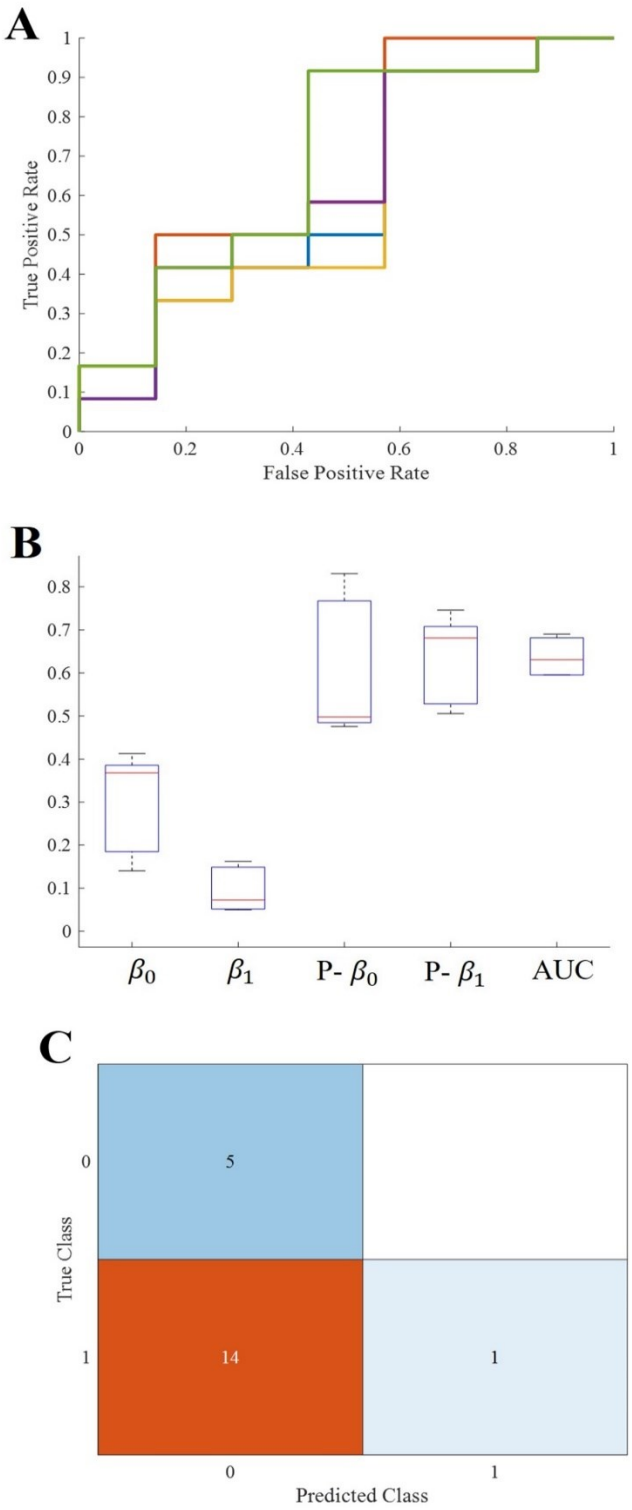

Figure 4.7 5-fold cross validation for clinical complexity with parameter feature variance of PF ratio. (A) ROC curves overlaid from all logistic regression models in the 1-fold validation scheme. Mean AUC was 0.6381. (B) Box plots of model statistics, including beta coefficients, p-values, and AUCs. (C) Final populated confusion from validation scheme, indicating an accuracy of 30%.

4.6 PF Ratios versus N1 Peaks

To determine the efficacy of our system metric over the current CCEP analysis through visual inspection of the N1 amplitude, we analyzed the correlation between PF ratio and peak amplitude as well as the confidence statistic for N1. The confidence statistic for N1 demonstrated slightly poorer performance in the classification of surgical outcomes than the PF ratio (Figure 4.4B). In the CCLow cases, one of the datasets (Patient 4) which has a successful surgical outcome has a CS < 1, while in the CCHigh case Patient 2, which had an unsuccessful surgical result, has a CS > 1 (Figure 4.4B). Additionally, the Pearson correlation between PF ratios and N1 peak amplitude for all datasets averaged 0.1515±0.1676, indicating little correspondence between the metrics,

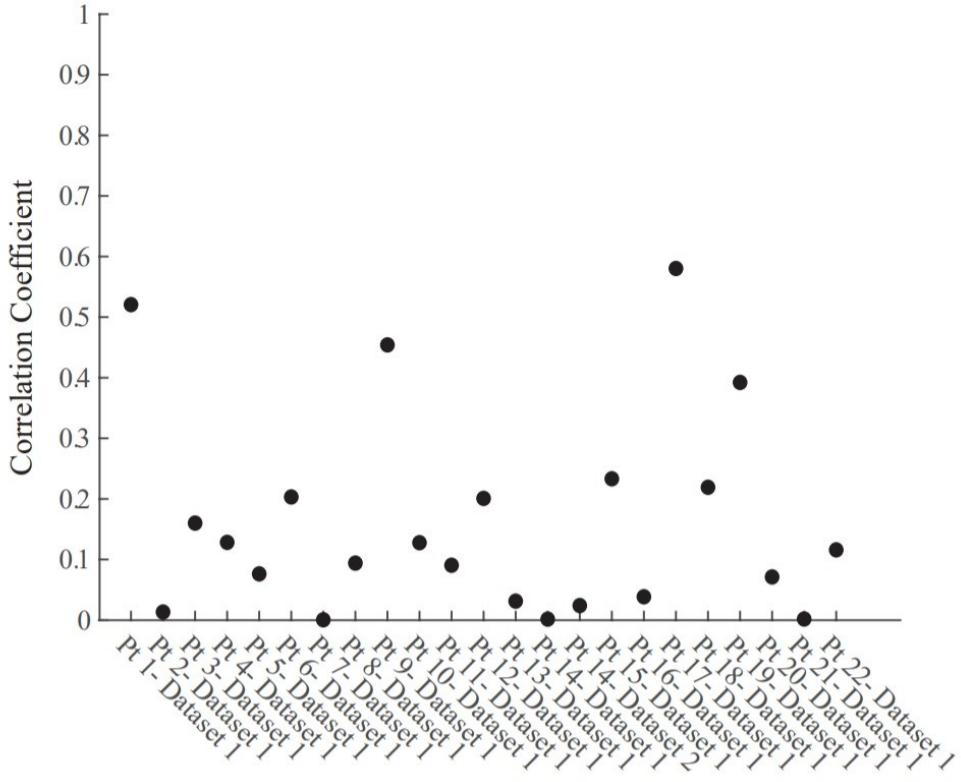

Figure 4.8 Pearson correlation between PF ratio and N1 peak for each dataset.

showing that the advantage of the PF ratio to the N1 peak is not due to any dependence. (Figure 4.5).

Chapter 5

Discussion

Patient specific dynamical network models were built from SPES data and analyzed for a population of medically refractory epilepsy patients that were admitted to the Johns Hopkins Hospital. These patients were admitted for the localization of their seizure network for the possibility of seizure freedom via surgical resection. As epileptic seizures are believed to result from a pathologically connected brain network with epileptic foci [77], we conjectured that the analysis of intracranial EEG data in response to stimulation in the context of dynamic networks would provide an advantage to current localization techniques that are based on passive iEEG. SPES provides an opportunity to actively perturb the brain, and then capture and analyze the rich dynamics of the iEEG network to localize the SOZ.

5.1 Hypothesis

We hypothesized that dynamical network models (DNMs), specifically transfer function models, can characterize the dynamics of brain network activity and provide quantitative metrics that can be used to help precisely and accurately localize the SOZ. We investigated properties of the transfer functions that reflected the epileptogenic nature of the EEG network. Specifically, we hypothesized that the peak system gain as defined by the H_∞ norm of the transfer function, a notion

that describes the amplification and spread of the CCEPs in the network, in conjunction with the cutoff frequency correlating to a sudden drop in magnitude, may reveal SOZ and early spread regions. We believe our approach will identify SOZ and early spread regions with greater accuracy than current visual and static assessment approaches alone, thereby improving surgical outcomes.

5.2 PF Ratios Correlate to Clinical Annotations

We hypothesized that the areas involved in the epileptogenic region, such as SOZ and EP, when stimulated, would produce the largest system gains and the biggest response drop-offs as compared to areas not involved in the epileptogenic network. We further conjectured that for those patients whose epilepsy was due to a lesion, had a focal onset, or originated solely in the temporal region (CCLow), the clinicians would be able to identify the SOZ accurately and completely. This would suggest that, in our models, those electrode pairs in the clinically annotated SOZ and EP, should have large peak gain values *and* small floor gain values, when compared to other electrode pairs. Therefore, we expected to see a higher degree of agreement between our PF ratios and the clinical annotations, resulting in a confidence statistic greater than or equal to 1. However, for those patients whose epilepsy was nonlesional, multifocal, and extratemporal, (CCHigh), we speculated that the clinicians had a more difficult time precisely locating the SOZ and early spread regions. Thus, we expected in these cases for our model ratios to have more variations and potential disagreements with the clinical annotations (highly variable CS), possibly highlighting areas that may have been overlooked or that could not be captured with the current localization methods. Our models may also be able to predict which patients will have surgical success and which will fail, depending on the level of disagreement between the model and the clinical annotations. A

larger discordance would indicate a more complex case and the increased likelihood of a failed outcome.

We explored the relationship between the ratio of the peak to floor gain of our transfer function models to regions of epileptogenic interest. Overall, we found that the patient cases classified of lower clinical complexity tended to have the highest ratio of system gains in the electrodes clinically marked as SOZ. If not in the SOZ, often the other higher ratio electrode pairs belonged to locations that were of interest, such as the EP. For example, Patient 13 had been classified as CCLow because the patient presented with a focal encephalomalacia of the inferior temporal lobe. This lesion, in conjunction with the patient's seizure semiology and iEEG recordings made the localization of the SOZ and early spread regions more straightforward for the clinicians.

On the other hand, as the clinical complexity increased, the discrepancies between the model PF ratios and the clinically annotated SOZs also increased. In Patient 14, the electrode pairs in the clinically annotated SOZ and EP yielded some of the smallest PF ratio values (Figure 4.2B). However, this patient has been admitted to the JHH EMU on two separate occasions for localization of seizure onset. During both stays, the clinicians were unable to localize the SOZ, requiring a third visit with the implantation of a grid. The inability to localize this patient's seizures implies that though there is disagreement between the clinical annotations and the PF ratios, our model may be identifying regions of interest that the clinicians were unable to identify through individual iEEG channel inspection.

5.3 Large Magnitude Drop Offs Correlate to Epileptogenic Regions

Studying the mean frequency responses of our systems, we explored properties that may indicate the epileptogenic zone. We observed that the frequency responses of the SOZ stimulated datasets in successful surgical outcomes, had not only some of the largest system gains, but also some of the quickest and biggest magnitude drops, especially when compared to their non-SOZ counterparts (Figure 4.3A). This difference became even more striking when comparing the mean SOZ stimulated datasets vs the mean non-SOZ stimulated datasets for a failed surgical outcome case. In this instance, the clinically annotated SOZ stimulated datasets had some of the smallest peak gains and some of the slower, smaller magnitude drop offs, while the non-SOZ stimulated datasets had a very peak gains and steep drop offs (Figure 4.3B). This indicates that the frequency response can capture the interactions and dynamics of the system and provide markers for the SOZ, but also potentially indicate frequencies at which seizures may be generated.

5.4 PF Ratios Reflect Surgical Outcomes

A true test for SOZ localization algorithms is in their ability to predict surgical outcomes. We defined a successful surgical outcome to be those patients with an Engel score or I & II, or if a responsive neurostimulation (RNS) device was implanted, an Engel score of III was considered a success. A failed surgical outcome was defined as those patients who had surgical resection or ablation and received an Engel score of III or IV. Patient 9 was categorized as CCLow and now has seizure freedom (ES I) (Figure 5.1A). The clinicians identified electrode pairs LTP01/02 and LTP02/03 as those they believed to be the SOZ (red). Our model revealed that LTP01/02 had the

highest PF ratio out of all electrode pairs. The regions denoted to be in the early spread (orange) also had some of the higher PF ratios, with our model highlighting electrode pair LHP03/04 as having the second highest PF ratio. The resected areas included the SOZ contacts LTP01/02 and LTP02/03, which had the two highest PF ratios. Given the surgical outcome of ES I, this demonstrates the agreement between our model and clinical annotations in patient cases of low clinical complexity and the correlation to successful surgical outcomes.

In unsuccessful surgical outcomes (ES III and ES IV), we hypothesized the highest PF ratios would be in regions not labeled as the SOZ. Patient 7 was a difficult case (CCHigh) who, despite a laser ablation at contact CINA1-2, had no improvement in their seizure frequency (ES IV) (Figure 5.1B). The low PF ratio in CINA1-2 indicates that our algorithm identified this region of the brain as non-epileptogenic. Moreover, our algorithm identified SENI3-4 and CIND8-9 as regions that may possibly show epileptogenicity due to the high PF ratios values in those regions.

There were instances where our model agreed with the clinical annotations resulting in a high confidence statistic, however, the surgical outcome did not result in seizure freedom. Outlier Patient 5 is a patient whose clinically annotated SOZ and EP contacts resulted in high PF ratios which would normally suggest a success (Figure 5.2). The regions that were resected were those in the SOZ pairs LPPS1/2 and LSPS1/2, which resulted in an unsuccessful surgical outcome (ES IV). However, despite the poor surgical results, the confidence statistic for this patient (Patient 5) was high (CS = 1.1412). Due to part of the SOZ (electrode pair LFP63/64) being located in a language area of the cortex, it was not surgically removed to prevent a functional deficit. The next highest PF ratio not resected was in the EP pair LFPG33/34, which was also located in the eloquent cortex (motor), making the tissue not viable for resection. Failing to remove the entire SOZ likely caused the failed outcome. This is just one of several examples demonstrating the complexity of

diagnosing and treating these patients and more importantly the difficulty of evaluating computational algorithms.

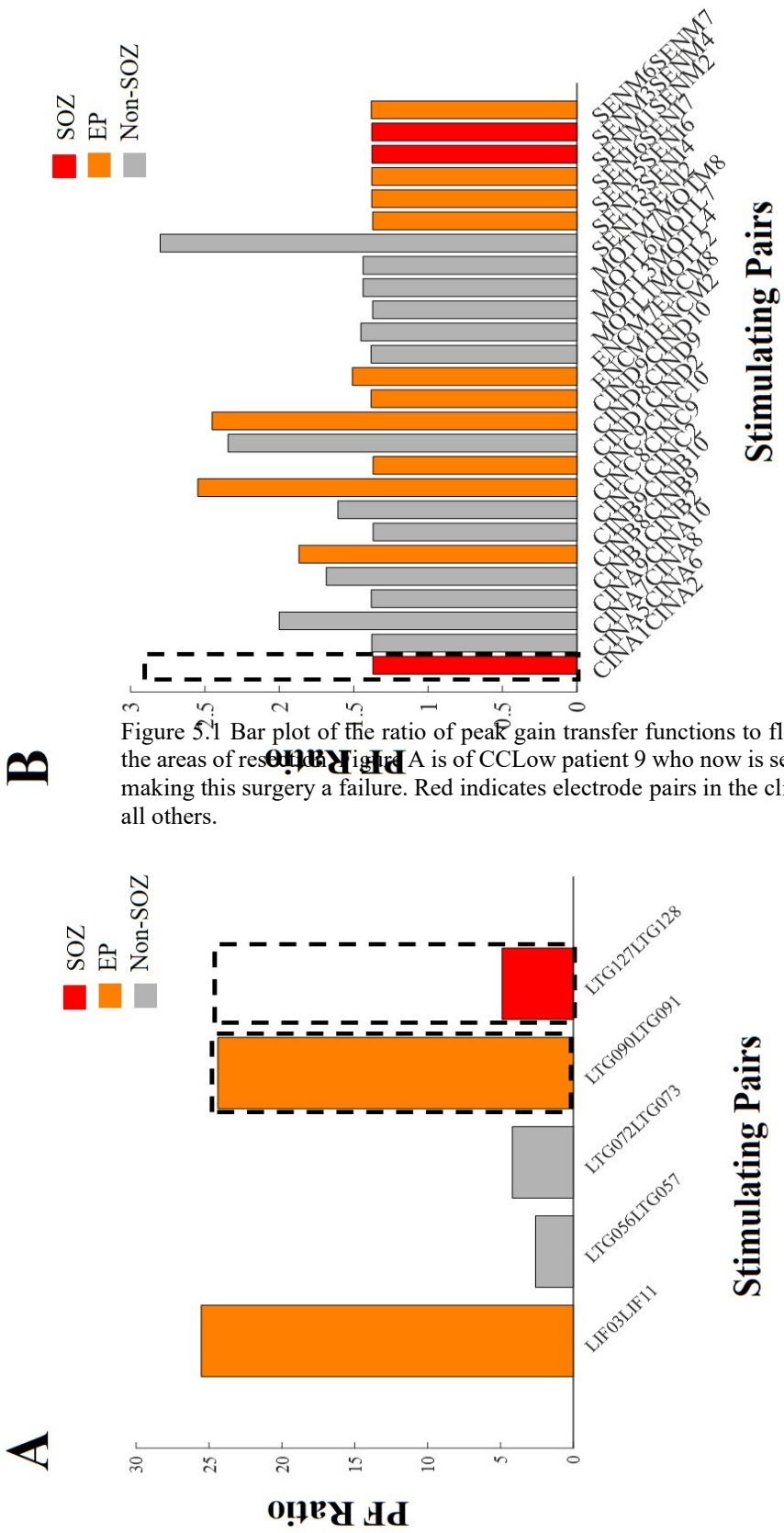

Figure 5.1 Bar plot of the ratio of peak gain transfer functions to floor gains for two patient datasets that hav
the areas of resection. Figure A is of CCLow patient 9 who now is seizure free (ESI), while figure B is of CCH
making this surgery a failure. Red indicates electrode pairs in the clinically annotated seizure onset zone (SOZ
all others.

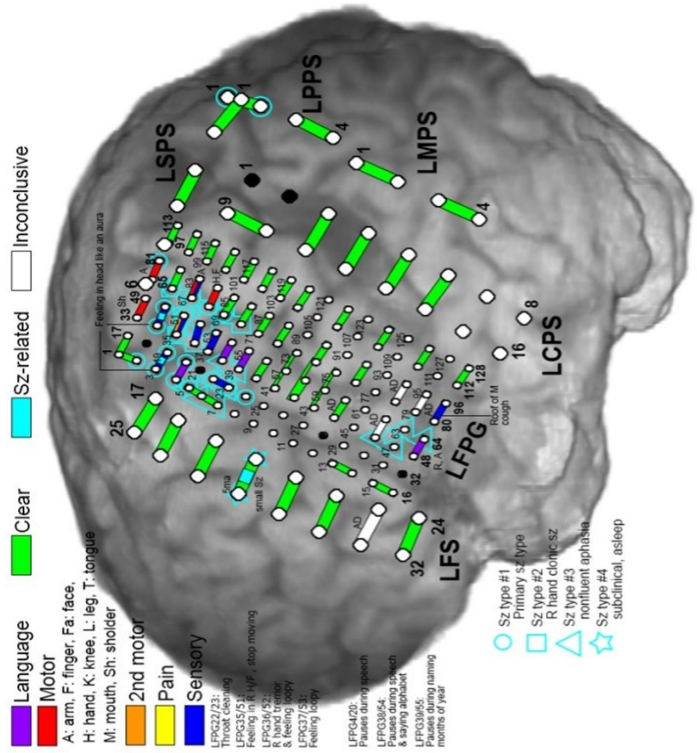

Figure 5.5 Bar plot of PF ratios for Patient 5 with a high confidence statistic value according to the model, t
dotted boxes represent the regions that were resected. Red indicates electrode pairs in the clinically annotated
spread (EP), yellow is irritative zone (IZ), and grey are all others. Regions with high PF ratios were not rese
possibly explaining the seizure persistence

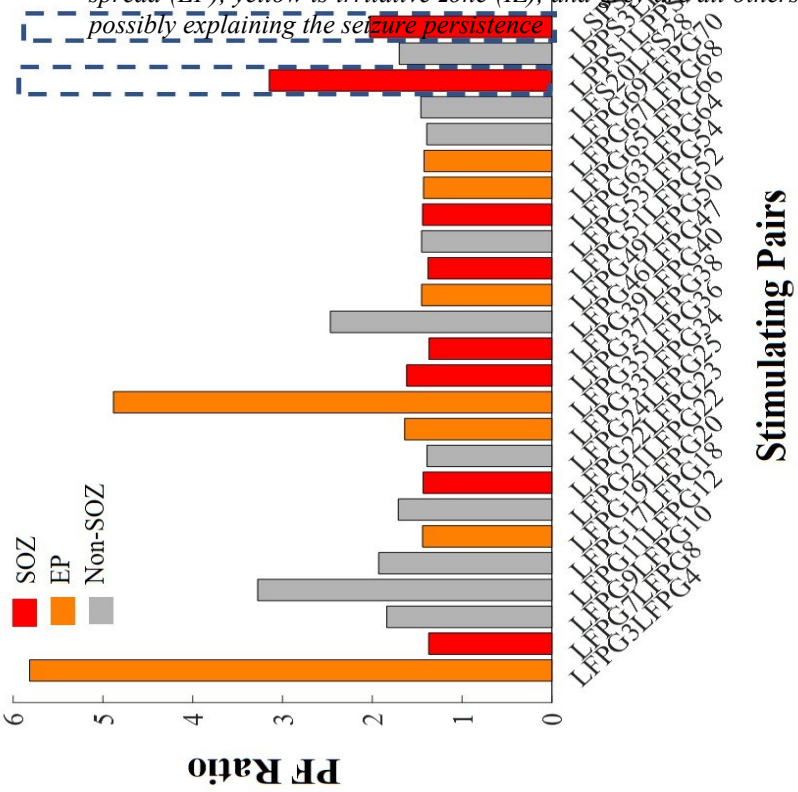

5.5 Study Limitations

The major limitation of this study is the low number of study subjects, particularly those with surgical outcomes. Extending this study to more patients with varying pathologies and epilepsy etiologies, particularly those with surgical outcomes, would increase the power of this study. The inclusion of more surgical outcome data would help to prove the efficacy of the PF ratio and its advantages over the N1 peak. There are also other properties of the transfer function models that need to be explored, such as the phase delay, bandwidth, and pole-zero locations. Potentially, analysis and inclusion of these additional metrics may help more accurately and fully characterize the epileptic network and show the advantage of using the PF ratio for localization of the SOZ, particularly in cases of high clinical complexity.

5.6 Future Work

In this study we have shown that in SOZ stimulated regions the peak of the frequency response is followed by a steep roll-off. This phenomenon suggests a resonance-like property of the network that could generate a seizure if the system is triggered by a periodic stimulation at a particular frequency. While this is a true for photosensitive epilepsy [84], our findings suggest the prevalence of resonance in all types of epilepsy. Therefore, in the future we plan on investigating the idea of resonance in the iEEG network more thoroughly and all the properties associated with it. Future work will also include designing an experimental study to test this notion of resonance by stimulating nodes at their corresponding resonance frequencies, as identified by our models, to see if seizures or epileptogenic activity are triggered.

Supplementary

Table 3.1 Patient Clinical Table

Summary of Patient Clinical Data. The following abbreviations were used: P = Patient; G = Gender; CC = Clinical Complexity; H = Clinical High Complexity; L = Clinical Low Complexity; ES = Engel Score; FocalA = Focal Awareness Seizure; FocalIA = Focal Impaired Awareness Seizures; TC = Tonic Clonic Seizures; MRgLiTT = MRI guided laser interstitial thermal therapy; RNS = Responsive Neurostimulator

P	G	Age	Seizure Type	MRI	SOZ	Surgery	Pathology	CC	ES	# of SOZ contacts	Total # of Stimulated Contacts
1	M	25	FocalA, FocalA to Bilateral TC	Non-lesional	Left frontal, involving the premotor and motor cortex	Resection	Non-specific, inflammatory changes	H	3	3	7
2	F	43	Focal_IA	Non-lesional	Left posterior basal temporal-occipital region	Resection	Normal	H	3	3	8
3	F	35	Focal-IAsensory Focal_IA	Cystic multilobulated cortically based mass in left temporal lobe	Left temporal	Resection	DNET versus oliogodendroglioma	H	2	1	5
4	F	18	FocalA to Bilateral TC	Subtle thickening in the right middle frontal gyrus	Right frontal	Resection	Cortical dysplasia	L	1	3	11
5	M	32	Focal-Asensory Focal-Amotor Focal_IA	Gliososis in the posterior superior left parietal lobe	Left superior parietal lobule	Resection	Cortical dysplasia	H	4	8	25

6	M	38	Focal_IA with occasional TC	Mild asymmetric thickening in the dorsal left para-hippocampal gyrus	Left mesial and para-hippocampal gyrus	MRgLiTT	N/A	L	1	4	5
7	F	32	Focal_IA	Left frontal encephalomalacia	Left posterior cingulate	MRgLiTT	N/A	H	4	3	26
8	F	27	Focal_IA	Bilateral occipital lissencephaly	Bilateral mesial temporal structures	RNS	N/A	H	3	8	13
9	F	24	Focal_IA	Left temporal encephalomalacia	Left temporal lobe	Resection	Non-specific, inflammatory changes	L	1	2	9
10	F	27	Focal_IA Focal_IA to Bilateral TC	Left periventricular heterotopia and left frontal encephalamalacia	Left inferior frontal region	Resection	Non-specific, inflammatory changes	H	1	4	19
11	F	51	Focal_IA Bilateral TC	Right MTS	Right mesial temporal structures	MRgLiTT	N/A	L	NA	2	6
12	M	48	Focal_IA	Periventricular bilateral nodular heterotopa and diffuse cortical dysgensis	Left mesial temporal structures	MRgLiTT	N/A	H	2	2	17
13	F	23	Focal_IA	Left temporal encephalomalacia	Left temporal lobe, mesial and neocortical	RNS	N/A	L	3	5	18
14A	F	23	Focal_IA	Non-lesional	Right posterior temporal region	Awaiting Surgery	N/A	H	NA	3	25
14B	F	23	Focal_IA	Non-lesional	Right posterior	Awaiting Surgery	N/A	H	NA	3	10

					temporal region						
15	M	32	Focal_IA with and without Bilateral TC	Non-lesional	Right temporal lobe (neocortex)	Awaiting Surgery	N/A	H	NA	1	9
16	M	32	Focal_IA	Right parietal encephalomalacia	Right temporal and parietal region	Awaiting Surgery	N/A	H	NA	5	14
17	M	19	Focal_IA with occasional TC	Non-lesional	Left mesial temporal structures	Awaiting Surgery	N/A	L	NA	4	17
18	F	35	Focal_IA	Right MTS	Bilateral mesial temporal structures	MRgLiTT	N/A	L	1	4	19
19	M	58	Focal_IA	Non-lesional	Left mesial temporal structures	Awaiting Surgery	N/A	H	NA	2	17
20	M	41	Focal_IA	Enlargement of the left amygdala	Left temporal neocortex	Awaiting Surgery	N/A	H	NA	5	18
21	F	32	Focal_A Focal_IA	Left occipital periventricular nodules	Left occipital and right posterior temporal region	Awaiting Surgery: Possible RNS	N/A	H	NA	2	15
22	F	53	Focal_IA with secondary generalization	Non-lesional	Left temporal lobe (temporal pole and mesial temporal structures	Awaiting Surgery	N/A	L	NA	7	25

References

[1] World Health Organization (2019). Epilepsy: a public health imperative. Geneva: World Health Organization; 2019. License: CC BY-NC-SA 3.0 IGO.

[2] Zack, M.M., Kobau, R., National and State Estimates of the Number of Adults and Children with Active Epilepsy—United States, 2015. MMWR Morb Mortal Wkly Rep 2017; 66:821-825. DOI: http://dx.doi.org/10.15585/mmwr.mm6631a1external_icon

[3] England, M. J., Liverman, C. T., Schultz, A. M., & Strawbridge, L. M. (2012). Summary: a reprint from epilepsy across the spectrum: promoting health and understanding. *Epilepsy currents*, *12*(6), 245–253. https://doi.org/10.5698/1535-7511-12.6.245

[4] Fisher, R.S., et al. ILAE official report: a practical clinical definition of epilepsy. Epilepsia. 2014 Apr;55(4):475-82. doi: 10.1111/epi.12550. Epub 2014 Apr 14. PMID: 24730690.

[5] Resendiz-Aparicio, J.C., Perez-Garcia, J.C., Olivas-Penas, E., Garcia-Cuevas, E., RoqueVillavicencio, Y., Hernandez-Hernandez, M., et al. "Clinical guideline: definition and classification of epilepsy.", Revista Mexicana de Neurociencia. 2019;20(2):63.

[6] Falco-Walter, J.J., Scheffer, I.E., Fisher, R.S. The new definition and classification of seizures and epilepsy. Epilepsy Res. 2018 Jan;139:73-79. doi: 10.1016/j.eplepsyres.2017.11.015. Epub 2017 Nov 28. PMID: 29197668.

[7] Perucca, E. An introduction to antiepileptic drugs. Epilepsia. 2005;46 Suppl 4:31-7. doi: 10.1111/j.1528-1167.2005.463007.x. PMID: 15968807.

[8] Goldenberg, M. M. (2010). Overview of drugs used for epilepsy and seizures: etiology, diagnosis, and treatment. *P & T : a peer-reviewed journal for formulary management*, *35*(7), 392–415.

[9] Brodie. M.J., Shorvon, S.D., Canger, R., Hal'oasz, P., Johannessen, S., Thompson, P., Wieser, H.G., and Wolf, P., "Commission on European affairs: Appropriate standards of epilepsy care across Europe," Epilepsia, vol. 38, no. 11, pp. 1245-1250, 1997.

[10] Berg, A.T.and Kelly, M.M, "Defining intractability: Comparisons among published definitions," Epilepsia, vol. 47, no. 2, pp. 431-436, 2006.

[11] Kwan, P.and Brodie, M.J., "Definition of refractory epilepsy: defining the indefinable?," The Lancet Neurology, vol. 9, no. 1, pp. 27-29, 2010.

[12] Begley,C.E., Famuluar, M., Annegers, J.F., Lairson ,D.R., Reynolds, T.F., Coan, S.,

Dubinsky, S., Newmark, M.E., Leibson, C., So, E.L., and Rocca, W.A.,"The cost of epilepsy in the United States: An estimate from population-based clinical and survey data." Epilepsia, vol. 41, no. 3, pp. 342-351.

[13] Begley, C.E. and Durgin, T.L., "The direct cost of epilepsy in the United States: A systematic review of estimates," Epilepsia, vol. 56, no. 9, pp. 1376-1387.

[14] Ferro, M.A., and Speechley, K.N., "Stability of latent classes in group-based trajectory modeling of depressive symptoms in mothers of children with epilepsy: an internal validation study using a bootstrapping procedure," Social Psychiatry and Psychiatric Epidemiology, vol. 48, pp. 1077-1086, Jul 2013.

[15] Murray, M.I., Halpern, M.T., and Leppik, I.E., "Cost of refractory epilepsy in adults in the USA," Epilepsy Research, vol. 23, no. 2, pp. 139-148, 1996.

[16] Bulacio, J.C., Jehi L., Wong, C., Gonzalez-Martinez, J., Kotagal, P., Nair, D., Naim, I., and Bingaman, W., "Longterm seizure outcome after resective surgery in patients evaluated with intracranial electrodes,", Epilepsia, vol. 53, no. 10, pp. 1722-1730, 2012.

[17] Gonzalez-Martinez, J.A., Srikijvilaikul, T., Nair, D., and Bingaman, W.E., "Long-term seizure outcome in reoperation after failure of epilepsy surgery,", Neurosurgery, vol. 60, no. 5, pp. 873-880, 2007

[18] Flanagan D, Valentin A, Garcia Seoane JJ, Alarcon G, Boyd SG. "Single-pulse electrical stimulation helps to identify epileptogenic cortex in children," Epilepsia 2009;50:1793–803.

[19] Valentin A, Alarcon G, Honavar M, Garcia Seoane JJ, Selway RP, Polkey CE, et al. "Single pulse electrical stimulation for identification of structural abnormalities and prediction of seizure outcome after epilepsy surgery: a prospective study," Lancet Neurol 2005;4:718–26.

[20] Iwasaki, M., Enatsu, R., Matsumoto, R., Novak. E., Thankappen, B., Piao, Z., et al, "Accentuated cortico-cortical evoked potentials in neocortical epilepsy in areas of ictal onset," Epileptic Disord 2010;12:292–302.

[21] Enatsu R, Piao Z, O'Connor T, Horning K, Mosher J, Burgess R, et al. "Cortical excitability varies upon ictal onset patterns in neocortical epilepsy: a cortico- cortical evoked potential study," Clin Neurophysiol 2012;123:252–60.

[22] van't Klooster MA, Zijlmans M, Leijten FS, Ferrier CH, van Putten MJ, Huiskamp GJ. "Time-frequency analysis of single pulse electrical stimulation to assist delineation of epileptogenic cortex," Brain 2011;134:2855–66.

[23] Keller, C. J., Honey, C. J., Entz, L., Bickel, S., Groppe, D. M., Toth, E., Mehta, A. D.

(2014). Corticocortical evoked potentials reveal projectors and integrators in human brain networks. *Journal of Neuroscience*, *34*(27), 9152–9163. https://doi.org/10.1523/JNEUROSCI.4289-13.2014

[24] Matsumoto, R., Nair, D. R., LaPresto, E., Najm, I., Bingaman, W., Shibasaki, H., & Lüders, H. O. (2004). Functional connectivity in the human language system: A cortico-cortical evoked potential study. *Brain*, *127*(10), 2316–2330. https://doi.org/10.1093/brain/awh246

[25] Keller, C. J., Honey, C. J., Mégevand, P., Entz, L., Ulbert, I., & Mehta, A. D. (2014). Mapping human brain networks with cortico-cortical evoked potentials. *Philosophical Transactions of the Royal Society B: Biological Sciences*, *369*(1653). https://doi.org/10.1098/rstb.2013.0528

[26] Matsumoto, R., Nair, D. R., LaPresto, E., Bingaman, W., Shibasaki, H., & Lüders, H. O. (2007). Functional connectivity in human cortical motor system: A cortico-cortical evoked potential study. *Brain*, *130*(1), 181–197. https://doi.org/10.1093/brain/awl257

[27] Enatsu, R., Gonzalez-Martinez, J., Bulacio, J., Kubota, Y., Mosher, J., Burgess, R. C., Nair, D. R. (2015). Connections of the limbic network: A corticocortical evoked potentials study. *Cortex*, *62*, 20–33. https://doi.org/10.1016/j.cortex.2014.06.018

[28] Lacruz, M. E., García Seoane, J. J., Valentin, A., Selway, R., & Alarcón, G. (2007). Frontal and temporal functional connections of the living human brain. *European Journal of Neuroscience*, *26*(5), 1357–1370. https://doi.org/10.1111/j.1460-9568.2007.05730.x

[29] Matsumoto, R., Nair, D. R., Ikeda, A., Fumuro, T., Lapresto, E., Mikuni, N., Lüders, H. O. (2012). Parieto-frontal network in humans studied by cortico-cortical evoked potential. *Human Brain Mapping*, *33*(12), 2856–2872. https://doi.org/10.1002/hbm.21407

[30] Almashaikhi, T., Rheims, S., Jung, J., Ostrowsky-Coste, K., Montavont, A., De Bellescize, J., Ryvlin, P. (2014). Functional connectivity of insular efferences. *Human Brain Mapping*, *35*(10), 5279–5294. https://doi.org/10.1002/hbm.22549

[31] Dionisio, S., Mayoglou, L., Cho, S. M., Prime, D., Flanigan, P. M., Lega, B., Nair, D. (2019). Connectivity of the human insula: A cortico-cortical evoked potential (CCEP) study. *Cortex*, *120*, 419–442. https://doi.org/10.1016/j.cortex.2019.05.019

[32] Kubota, Y., Enatsu, R., Gonzalez-Martinez, J., Bulacio, J., Mosher, J., Burgess, R. C., & Nair, D. R. (2013). In vivo human hippocampal cingulate connectivity: A corticocortical evoked potentials (CCEPs) study. *Clinical Neurophysiology*, *124*(8), 1547–1556. https://doi.org/10.1016/j.clinph.2013.01.024

[33] Mégevand, P., Groppe, D. M., Bickel, S., Mercier, M. R., Goldfinger, M. S., Keller, C. J., Mehta, A. D. (2017). The Hippocampus and Amygdala Are Integrators of Neocortical Influence: A CorticoCortical Evoked Potential Study. *Brain Connectivity*, *7*(10), 648–660. https://doi.org/10.1089/brain.2017.0527.

[34] Matsumoto, R., Kunieda, T., & Nair, D. (2017). Single pulse electrical stimulation to probe functional and pathological connectivity in epilepsy. *Seizure*, *44*, 27–36. https://doi.org/10.1016/j.seizure.2016.11.003

[35] Enatsu, R., Piao, Z., O'Connor, T., Horning, K., Mosher, J., Burgess, R., Nair, D. (2012). Cortical excitability varies upon ictal onset patterns in neocortical epilepsy: A cortico-cortical evoked potential study. *Clinical Neurophysiology*, *123*(2), 252–260. https://doi.org/10.1016/j.clinph.2011.06.030

[36] Zhang, N., Zhang, B., Rajah, G. B., Geng, X., Singh, R., Yang, Y., Sun, W. (2018). The effectiveness of cortico-cortical evoked potential in detecting seizure onset zones. *Neurological Research*, *40*(6), 480–490. https://doi.org/10.1080/01616412.2018.1454092

[37] Enatsu, R., Jin, K., Elwan, S., Kubota, Y., Piao, Z., O'Connor, T., Nair, D. R. (2012). Correlations between ictal propagation and response to electrical cortical stimulation: A cortico-cortical evoked potential study. *Epilepsy Research*, *101*(1–2), 76–87. https://doi.org/10.1016/j.eplepsyres.2012.03.004

[38] Lega, B., Dionisio, S., Flanigan, P., Bingaman, W., Najm, I., Nair, D., & Gonzalez-Martinez, J. (2015). Cortico-cortical evoked potentials for sites of early versus late seizure spread in stereoelectroencephalography. *Epilepsy Research*, *115*, 17–29. https://doi.org/10.1016/j.eplepsyres.2015.04.009

[39] Kokkinos, V., Alarcón, G., Selway, R. P., & Valentín, A. (2013). Role of single pulse electrical stimulation (SPES) to guide electrode implantation under general anaesthesia in presurgical assessment of epilepsy. *Seizure*, *22*(3), 198–204. https://doi.org/10.1016/j.seizure.2012.12.012

[40] Nayak, D., Valentín, A., Selway, R. P., & Alarcón, G. (2014). Can single pulse electrical stimulation provoke responses similar to spontaneous interictal epileptiform discharges? *Clinical Neurophysiology*. https://doi.org/10.1016/j.clinph.2013.11.019

[41] Valentin, A., Anderson, M., Alarcón, G., García-Seoane, J. J., Selway, R., Binnie, C. D., & Polkey, C. E. (2002). Responses to single pulse electrical stimulation identify epileptogenesis in the human brain in vivo. *Brain*, *125*(8), 1709–1718. https://doi.org/10.1093/brain/awf187

[42] Flanagan, D., Valentín, A., García Seoane, J. J., Alarcón, G., & Boyd, S. G. (2009). Single-pulse electrical stimulation helps to identify epileptogenic cortex in children. *Epilepsia*, *50*(7), 1793–1803. https://doi.org/10.1111/j.1528-1167.2009.02056.x

[43] Valentín, A., Alarcón, G., García-Seoane, J. J., Lacruz, M. E., Nayak, S. D., Honavar, M., Polkey, C. E. (2005). Single-pulse electrical stimulation identifies epileptogenic frontal cortex in the human brain. *Neurology*, *65*(3), 426–435. https://doi.org/10.1212/01.wnl.0000171340.73078.c1

[44]Valentín, Antonio, Alarcón, G., Honavar, M., García Seoane, J. J., Selway, R. P., Polkey, C. E., & Binnie, C. D. (2005). Single pulse electrical stimulation for identification of structural abnormalities and prediction of seizure outcome after epilepsy surgery: A prospective study. *Lancet Neurology*, *4*(11), 718–726. https://doi.org/10.1016/S1474-4422(05)70200-3

[45] Kobayashi, K., Matsumoto, R., Matsuhashi, M., Usami, K., Shimotake, A., Kunieda, T., Ikeda, A. (2017). High frequency activity overriding cortico-cortical evoked potentials reflects altered excitability in the human epileptic focus. *Clinical Neurophysiology*, *128*(9), 1673–1681. https://doi.org/10.1016/j.clinph.2017.06.249

[46] Mouthaan, B. E., Van't Klooster, M. A., Keizer, D., Hebbink, G. J., Leijten, F. S. S., Ferrier, C. H., Huiskamp, G. J. M. (2016). Single Pulse Electrical Stimulation to identify epileptogenic cortex: Clinical information obtained from early evoked responses. *Clinical Neurophysiology*, *127*(2), 1088–1098. https://doi.org/10.1016/j.clinph.2015.07.031

[47] Davis, T. S., Rolston, J. D., Bollo, R. J., & House, P. A. (2018). Delayed high-frequency suppression after automated single-pulse electrical stimulation identifies the seizure onset zone in patients with refractory epilepsy. *Clinical Neurophysiology*, *129*(11), 2466–2474. https://doi.org/10.1016/j.clinph.2018.06.021

[48] Jacobs, J., Zijlmans, M., Zelmann, R., Olivier, A., Hall, J., Gotman, J., & Dubeau, F. (2010). Value of electrical stimulation and high frequency oscillations (80-500 Hz) in identifying epileptogenic areas during intracranial EEG recordings. *Epilepsia*, *51*(4), 573–582. https://doi.org/10.1111/j.1528-1167.2009.02389.

[49] Van'T Klooster, M. A., Zijlmans, M., Leijten, F. S. S., Ferrier, C. H., Van Putten, M. J. A. M., & Huiskamp, G. J. M. (2011). Time-frequency analysis of single pulse electrical stimulation to assist delineation of epileptogenic cortex. *Brain*, *134*(10), 2855–2866. https://doi.org/10.1093/brain/awr211

[50] Van 't Klooster, M. A., van Klink, N. E. C., van Blooijs, D., Ferrier, C. H., Braun, K. P. J., Leijten, F. S. S., … Zijlmans, M. (2017). Evoked versus spontaneous high frequency oscillations in the chronic electrocorticogram in focal epilepsy. *Clinical Neurophysiology*. https://doi.org/10.1016/j.clinph.2017.01.017

[51] Donos, C., Mîndruţă, I., Malîia, M. D., Raşină, A., Ciurea, J., & Barborica, A. (2017). Co-occurrence of high-frequency oscillations and delayed responses evoked by intracranial electrical stimulation in stereo-EEG studies. *Clinical Neurophysiology*, *128*(6), 1043–1052. https://doi.org/10.1016/j.clinph.2016.11.028

[52] Boido, D., Kapetis, D., Gnatkovsky, V., Pastori, C., Galbardi, B., Sartori, I., De Curtis, M. (2014). Stimulus-evoked potentials contribute to map the epileptogenic zone during stereo-EEG presurgical monitoring. *Human Brain Mapping*, *35*(9), 4267–4281. https://doi.org/10.1002/hbm.22516

[53] Van Blooijs, D., Leijten, F. S. S., van Rijen, P. C., Meijer, H. G. E., & Huiskamp, G. J. M.

(2018). Evoked directional network characteristics of epileptogenic tissue derived from single pulse electrical stimulation. *Human Brain Mapping*, *39*(11), 4611–4622. https://doi.org/10.1002/hbm.24309

[54] Zhao, C., Liang, Y., Li, C., Gao, R., Wei, J., Zuo, R., Zhang, X. (2019). Localization of epileptogenic zone based on cortico-cortical evoked potential (CCEP): A feature extraction and graph theory approach. *Frontiers in Neuroinformatics*, *13*(April), 1–9. https://doi.org/10.3389/fninf.2019.00031

[55] L¨uders, H. and U., S.S., "Epilepsy surgery in patients with malformations of cortical development," Current Opinion in Neurology, vol. 19, pp. 169-174, Apr 2006.

[56] Sheikh, S., Thompson, N., Bingaman, W., Gonzalez Martinez, J., Najm, I., and Jehi, L, "Redefining success in epilepsy surgery: The importance of relative seizure reduction in patient reported quality of life," Epilepsia, pp 2078-2085, Aug 2019.

[57] Farahani, F.V., Karwowski, W., Lighthall, N.R., "Application of Graph Theory for Identifying Connectivity Patterns in Human Brain Networks: A Systematic Review," Frontiers in neuroscience. 2019;13:585.

[58] Bernhardt, C., Bonilha, L., and Gross, D. W., "Network analysis for a network disorder: The emerging role of graph theory in the study of epilepsy," Epilepsy Behav., vol. 50, pp. 162–170, 2015.

[59] Rubinov, M. and Sporns, O. (2010). Complex network measures of brain connectivity: uses and interpretations. *Neuroimage.* 52, 1059-1069. doi: 10.1016/j.neuroimage.2009.10.003.

[60] Bullmore, E.T., and Bassett, D.S. (2011). Brain graphs: graphical models of the human brain connectome. *Annu. Rev. Clin. Psychol.* 7, 113-140. doi: 10.1146/annurev-clinpsy-040510-143934.

[61] Zhao, C., Liang,Y., Li, C. Gao, R., Wei, J. Zuo, R., Zhong, Y., Ren, Z., Geng, X., Zhang, G., and Zhang, X., Localization of Epilpetogenic Zone Based on Cortico-Cortical Evoked Potential (CCEP)L A Feature Extraction and Graph Theory Approach. *Frontiers in Neuroinformatics*. Vol. 13, doi: 10.3389/fninf.2019.00031

[62] Izadian, A. (2019). *Fundamentals of modern electric circuit analysis and filter synthesis: A transfer function approach*. Cham, Switzerland: Springer.

[63] Rugh, W. J. (1996). *Linear system theory* (2nd ed.). Upper Saddle River, NJ: Prentice Hall.

[64] Hespanha, J. P. (2018). *Linear systems theory*. Princeton, NJ: Princeton University Press.

[65] Gotz-Trabert, K., Hauck, C., Wagner, K., Fauser, S., Schulze- Bonhage, A., 2008. Spread of ictal activity in focal epilepsy. Epilepsia 49, 1594-1601.

[66] Engel, Jerome (1993). *Surgical Treatment of the Epilepsies.* Lippincott Williams & Wilkins. ISBN 0-88167-988-7.

[67] Bulacio, J. C., Chauvel, P., and McGonigal, A, "Stereoelectroencephalography: Interpretation," Journal of Clinical Neurophysiology, Dec 2016.

[68] Ryvlin, P., Cross, J. H., & Rheims, S., "Epilepsy surgery in children and adults," The Lancet Neurology, 2014.

[69] Vakharia, V. N., Duncan, J. S., Witt, J. A., Elger, C. E., Staba, R., and Engel, J., "Getting the best outcomes from epilepsy surgery," Annals of Neurology, 2018.

[70] Chen, H., Agostini, M., Ding, K., Gupta, P., Madden, C., Mickey, B., and Modur, P, "Predictors of Seizure Recurrence and Longitudinal Outcome after Epilepsy Surgery," Neurology vol 80, pp04, 2013.

[71] Blackrock Microsystems LLC, Salt Lake City, UT

[72] MATLAB (2019). *9.7.0.1296695 (R2019b) Update 4,* [computer program], The Mathworks, Inc., Natick, Massachusetts 2019.

[73] Kamali, G., Smith, R.J., Hays, M., Coogan, C. G., Crone, N.E., Sarma, S.V., Kang, J.Y. (2020) Localizing the seizure onset zone from single pulse electrical stimulation responses using transfer function models, *42nd Annual International Conference of the IEEE Engineering in Medicine and Biology Society*: *Enabling Innovative Technologies for Global Healthcare, EMBC 2020.* Institute of Electrical and Electronics Engineer pp. 2524-2527. 917594 (Proceedings of the Annual International Conference of the IEEE Engineering in Medicine and Biology Society, EMBS; Vol. 2020-July).

[74] Smith, R.J., Kamali, G., Hays, M., Coogan, C. G., Crone, N.E., Sarma, S.V., and Kang, J.Y..(2020) Localizing the seizure onset zone from single pulse electrical stimulation responses using transfer function models, *42nd Annual International Conference of the IEEE Engineering in Medicine and Biology Society*: *Enabling Innovative Technologies for Global Healthcare, EMBC 2020.* Institute of Electrical and Electronics Engineer Inc. pp. 2528-2531.9176697. (Proceedings of the Annual International Conference of the IEEE Engineering in Medicine and Biology Society, EMBS; Vol. 2020-July).

[75] Proctor, J. L., Brunton, S. L., and Kutz, J. N., "Dynamic mode decomposition with control," *SIAM J. Appl. Dyn. Syst.*, vol. 15, no. 1, pp. 142–161, 2016.

[76] Kamali, G., Smith, R.J., Hayes, M., Coogan, C.G., Crone, N.E., Kang, J.Y. and Sarma, S.V. (2020), Transfer Function Models for the Localization of Seizure Onset Zone from Cortico-Cortical Evoked Potentials. Front. Neurol. 11:579961. doi:10.3389/fneur.2020.579661

[77] Li, A., Inati, S., Zaghlou K., Sarma, S., "Fragility in Epileptic Networks: The Epileptogenic

Zone," 2017 *American Control Conference*, pp 2817-2822, May 24-26, 2017.

[78] Sritharan, D. and Sarma, S.V., "Fragility in dynamic networks: applications to neural networks in the epileptic cortex. *Neural Computation*, 2014 vol 26 No 10.

[79] Nilsson, J. W., & Riedel, S. A. (2015). *Electric circuits*. Harlow, NJ: Pearson Education.

[80] Khambhati, A. N., Davis, K. A., Oommen, B. S., Chen, S. H., Lucas, T. H., Litt, B., & Bassett, D. S. (2015). Dynamic Network Drivers of Seizure Generation, Propagation and Termination in Human Neocortical Epilepsy. *PLoS Computational Biology*, *11*(12), 1–19. https://doi.org/10.1371/journal.pcbi.1004608

[81] Blume, W.T., 2009. Clinical intracranial overview of seizure syn- chrony and spread. Can. J. Neurol. Sci. 36 (Suppl. 2), 55-57.

[82] Chagnac-Amitai, Y., Connors, B.W., 1989. Horizontal spread of synchronized activity in neocortex and its control by GABA- mediated inhibition. J. Neurophysiol. 61, 747-758.

[83] Connors, B.W., Pinto, D.J., Telfeian, A.E., 2001. Local pathways of seizure propagation in neocortex. Int. Rev. Neurobiol. 45, 527-546.

[84] Martins da Siliva, A., Leal, "Photosensitivity and epilepsy: Current concepts and perspectives-A narrative review," *Seizure*. Vol 50 pp 209-218, 2017 Aug., doi: 10.1016/j.seizure.2017.04.0001.PMID 285 32712.

Curriculum Vitae

Golnoosh Kamali

110 W. 39th St
Apt 1216
Baltimore, MD 21210

Email:golnoosh.kamali@gmail.com
Phone: (219) 730-0377

EDUCATION

2020 **The Johns Hopkins University**
Doctor of Philosophy, Department of Electrical & Computer Engineering

2016 **The Johns Hopkins University**
Master of Science in Engineering, Department of Electrical & Computer Engineering

2012 **The University of Oklahoma**
Master of Science, Department of Electrical & Computer Engineering

2011 **The University of Oklahoma**
Bachelor of Science, Department of Electrical Engineering
Degree earned with Academic Distinction, Minor in Mathematics

PROFESSIONAL EXPERIENCE

The Johns Hopkins University

09/2019-present *Graduate Research Assistant, Department of Electrical & Computer Engineering, Neuromedical Control Systems Lab*
Creating dynamical network models of iEEG evoked responses to help clinicians better localize the seizure onset zone in epileptic patients. Building patient specific input-output models and using principles of linear systems theory to help focalize the seizure and its path of propagation.

AIDAR Health

Summer 2019 *Engineering Intern*
Conducted user studies at the Johns Hopkins Hospital to test the medical device MouthLab. Interaction with patients, doctors, and other medical professions, providing as the technical expert and consultant. Troubleshooting software and hardware issues with the device. Data analysis and data management.

The Johns Hopkins University

09/2017-05/2019 *Graduate Research Assistant, Department of Electrical & Computer Engineering, Machine Biointerface Lab*
Research in computational neural modeling, specifically building computational models of neurons to better understand how ionic direct current can be used to not only excite but also inhibit the propagation of action potentials for applications such as suppression of chronic pain, asthma attacks, and restoring the vestibular system.

Summer 2015 *Research Assistant, Air Force Summer Faculty Fellowship Program, Kirtland Airforce Base, Albuquerque, NM*
Worked in the Space Vehicles Directorate division on a control-theoretic framework for spacecraft autonomy, evaluating 20 different methodologies available for the synthesis and analysis of hybrid systems based on abstractions and created a database highlighting these methodologies in an easy to read manner.

08/2012-12/2015 *Graduate Research Assistant, Department of Electrical & Computer Engineering*
Research in control theory, specifically hybrid systems and their connections to game theory. Modeled hybrid systems using finite state machines to solve an optimization problem, whose solution resulted in a full-state feedback control law. Extended our models to nondeterministic finite state machines and analyzed the relationships between finite state machines in control theory and automata in computer science.

The University of Oklahoma

02/2012-05/2012 *Graduate Assistant on Special Projects, Dept of Electrical & Computer Engineering*
Helped create surveys for recent alumnus from the ECE Dept of OU. Used the data collected to help with the revision of the curriculum criteria to meet ABET requirements.

08/2011-01/2012 *Lab Technician for ECE Department*
Performed lab duties for the Electronics Lab, Circuits Lab I, and Capstone Lab. Managed lab equipment and performed duties for numerous lab classes.

08/2010-05/2011 *Undergraduate/Graduate Research Assistant Computational Imaging Laboratory*
Worked with a PhD student on her dissertation dealing with the correlation between brain wave signals and determining the onset of mental fatigue. Analyzed data and performed correlating IRB approved experiments.

05/2009-08/2011 *Student Supervisor Library Assistant,* Bizzell Memorial Library
Managed books, documents for patrons, and shipments in the Interlibrary Loan Department/Document Delivery area of the Access Service Department. Supervised a team of student workers.

Purdue University Northwest

08/2007-08/2008 *Computer Technician*
Desktop support technician who worked and coordinated moves campus wide as well as supporting faculty/staff computing needs.

TEACHING & MENTORING EXPERIENCE

The Johns Hopkins University

Fall 2020 *Teaching Assistant for Information Theory, Department of Electrical & Computer Engineering*
Supplementing the class with outside help for the students such as holding office hours once a week, answering questions on Piazza, and grading homework. Providing the professor with ideas and assistance on ways to improve the course by helping to create new quiz and exam questions, programming assignments, and suggestions to enhance virtual learning.

Fall 2020 *Graduate Mentor for Womnx Mentoring Pilot Program, Johns Hopkins University*
Graduate student mentor to a Johns Hopkins Undergraduate female in the Whiting School of Engineering in the Womnx Mentoring Whiting program. A mentorship program built to support women of all levels in the Whiting School of Engineering at Johns Hopkins University. Meet with my mentee at least once a month to discuss any topics that are of concern to them, helping them navigate their time at Hopkins as a women pursuing an engineering degree by providing guidance, skills, resources, and my own personal experiences as a women in STEM.

Anne Arundel Community College

Fall 2016-Fall 2017 *Instructor in the Department of Engineering*
Taught and developed classes mainly in the Engineering Transfer Program, particularly in the program of electrical and computer engineering. Developing and teaching classes such

as Introduction to Engineering Design, Digital Logic Design with lab, and Introduction to Programming. Duties included but not limited to holding office hours, serving on committees, student advisement, service during student and faculty orientation, attending conferences and workshops to enhance my skill set, and community outreach, particularly to those underrepresented in STEM.

Fall 2016-Spring 2017 *Mentor in Engineering Scholars Program*
A faculty mentor/advisor to five students in the Engineering Scholars Program at Anne Arundel Community College. A merit & financial based program offering scholarships to students who are pursuing a degree in engineering at AACC. Met with the students at least twice a week to discuss how they are doing in classes, provide them with skills to be successful in not only school but also life, and to provide them guidance and a listening ear.

The Johns Hopkins University

Fall 2015 *The Game for Control for Systems that Jump & Flow: An Introduction to Feedback Control, Hybrid Systems, and Games*
Created and taught a Hopkins Engineering and Research Tutorials (HEART) class. The goal of the seminar class was for the students to leave with a better understanding and appreciation for control theory, the connections to game theory, and gaining an interest in pursuing research opportunities in the STEM fields, particularly electrical engineering.
Course Evaluation: 4.0/5.0 Teacher Evaluation: 4.14/5.0

Summer 2014 *Mentored a High School Student from the Bryn Mawr School for Girls*
Mentored a high school student to help her utilize a top-down design methodology for problem solving doing so while teaching her the basics of game theory, all while finding ways to spark her interest in the STEM fields, particularly electrical engineering.

The University of Oklahoma

02/2012-05/2012 *Graduate Teaching Assistant for Advanced Electronics*
Supplemented the class with outside help for the students such as holding office hours twice a week, grading assignments, and helping with class projects.

08/2011-01/2012 *Graduate Teaching Assistant for Energy Conversion & Electronics*
Supplemented the classes with outside help for the students such as holding office hours twice a week, grading assignments, and helping with class projects.

PRESENTATIONS, PROCEEDINGS, AND PAPERS

G. Kamali, R.J. Smith, M. Hayes, C. Coogan, N.E. Crone, J..Y.Kang, and S.V. Sarma (2020), Transfer Function Models for the Localization of Seizure Onset Zone from Cortico-Cortical Evoked Potentials. Front. Neurol. 11:579961. doi:10.3389/fneur.2020.579661

G. Kamali, R.J. Smith, M. Hayes, C. Coogan, N.E. Crone, S.V. Sarma, and J.Y. Kang, "Localizing the seizure onset zone from single pulse electrical stimulation responses using transfer function models," 2020 42nd Annual International Conference of the IEEE Engineering in Medicine and Biology Society (EMBC), Canada, July 20-24.

R.J. Smith, **G. Kamali**, M. Hayes, C. Coogan, N.E. Crone, S.V. Sarma, and J.Y. Kang, "State-space models of evoked potentials to localize the epileptogenic zone," in proceedings, 2020 42nd Annual International Conference of the IEEE Engineering in Medicine and Biology Society (EMBC), Canada, July 20-24.

G. Kamali and G.Y. Fridman, "Analysis of Axon Compartmentalization in the Modeling of Direct Current Induced Conduction Block," Poster session presented at the 2018 North American Neuromodulation Society (NANS) Conference, Las Vegas, Nevada.

M. Rawhouser, **G. Kamali**, B. Baran, "Promoting engagement and success in an introductory discipline-specific course," Talk session presented at the 2018 Association of Faculties for the Advancement of Community College (AFACCT) Conference, Arnold, Maryland.

G. Kamali, "Second Friday Engineering Series Seminar: Adventures in Electrical Engineering Research," AACC Engineering Department & AACC Engineering Scholar Program, October 2016.

X. Zhang, **G. Kamali**, and D.C. Tarraf, "Optimizing the scaling parameter for ρ/μ approximation based control synthesis," Proceedings of the IEEE Multi-Conference on Systems and Control, Antibes, France, October 2014, pp.1527-1532.

HONORS & AWARDS

The Johns Hopkins University

03/08/2016	*Johns Hopkins High Table,* Invited by freshman class as a faculty member
08/2012-05/2013	*Ferdinand Hamburger, Jr. Fellowship in Electrical Engineering*

The University of Oklahoma

Spring 2011	*Director's Leadership Award*, School of Electrical & Computer Engineering
Fall 2010	*Who's Who Among Students in American Universities and Colleges*
Spring 2010	*Director's Service Award*, School of Electrical & Computer Engineering
08/2009-05/2011	*Clyde Farrar Endowment Scholarship*, School of Electrical & Computer Engineering
08/2009-05/2010	*Majorie Haskell Engineering Scholarship*, School of Electrical & Computer Engineering
08/2008-05/2011	*Transfer Scholarship*
08/2008-05/2011	*The University of Oklahoma Honors Program*
08/2008-05/2011	*Dean's List*

Purdue University Northwest

Spring 2008	*Recipient of LSAMP Grant Award*
08/2007-05/2008	*Best and Brightest Scholarship*
08/2007-05/2008	*Honors Program*
08/2007-05/2008	*Dean's List*

COMPUTER SKILLS

- *Microsoft Office*
  - Word; PowerPoint; Excel; Outlook
- *Operating Systems*
  - Windows 10/8/7/Vista/XP/2000/98/95
  - MacOS X
- *Computing Software*
  - MATLAB; LaTeX; Simulink; LabVIEW; NEURON; C; SolidWorks;

LANGUAGE SKILLS

- *English*: Fluent/Native Proficiency
- *Farsi*: Fluent/Native Proficiency
- *Spanish*: Elementary Proficiency

PROFESSIONAL SOCIETIES & STUDENT ORGANIZATIONS

Fall 2020	Womnx Mentoring Whiting, *Graduate Mentor*
Fall 2017-Present	Women of Whiting (WOW), *member* *Co-President* (Fall 2019-present)
Fall 2018-Present	JHU Translational Neuroengineering Technologies Network (JHUTNT), *member* *Student Leader and Webmaster* (Fall 2018-present)

Fall 2018-Spring 2019	JHU Library Student Advisory Committee *Graduate Student Member*
Fall 2015-Spring 2016	Graduate Representative Organization (GRO) *ECE Graduate Department Representative*
2009-Present	Eta Kappa Nu (HKN), *member* *Vice President* (Fall 2010-Spring 2011) *Recording Secretary* (Fall 2009-Spring 2010)
2009-Present	Institute of Electrical and Electronics Engineers (IEEE), *member* *Secretary* (Fall 2010-Spring 2011)
2008-Present	Tau Beta Pi (TBP), *member*
2007-2012	Society of Women Engineers (SWE), *member*
2008-2011	Phi Sigma Pi (National Honors Fraternity), *member* *President* (Spring 2010-Fall 2010) *Secretary* (Fall 2009)
Fall 2009	OU Student Martial Arts Association, *Secretary/Historian*
2008-Present	Golden Key Chapter (International Honor Society), *member*

VOLUNTEER & COMMUNITY SERVICE

02/25/2020	ECE Graduate Student Association (GSA) National Engineering Week at Barclay Elementary School-*Volunteer*
02/08/2020	L'Oreal Girl Scout STEM roller coaster event at Johns Hopkins University-*Volunteer and Role Model*
11/2019	SABES Elementary School-*Mentor*
04/06/2019	Women in STEM Symposium at Johns Hopkins University-*Planning committee member & Volunteer*
03/23/2019	L'Oreal Girl Scout STEM roller coaster event at Johns Hopkins University-*Volunteer and Role Model*
03/14/2019	Barclay STEM Expo-*Volunteer*
05/15/2018	SABES Spring STEM Showcase-*Volunteer*
04/19/2018	Barclay Science & Engineering Expo at Barclay Elementary/Middle School-*Volunteer*
04/07/2018	Women in STEM Symposium at Johns Hopkins University-*Volunteer*
Spring 2018	L'Oréal Girl Scout STEM roller coaster event at Johns Hopkins University- *Marketing Team Leader*
Spring 2017	FIRST LEGO league robotics competition at University of Maryland Baltimore County- *Referee*
Spring 2017	Served on the Faculty Search Committee for the Engineering Department at Anne Arundel Community College

Fall 2016	FIRST LEGO league robotics competition at Anne Arundel Community College- *Referee*
Spring 2015-Spring 2016	5th grade *math mentor/tutor* at the Henderson-Hopkins Middle School
06/20/2011	Engineering GLAMS Camp at OU-*Volunteer*
06/16/2011	BP Engineering Academy Camp at OU-*Volunteer*
06/15/2011	BP DEVAS Camp at OU-*Volunteer*
06/07/2011	Shell Passport to Engineering Camp at OU-*Volunteer*
04/04/2011	Tour guide for prospective ECE Professor at OU
April 2011	Big Event Day of Community Service at OU-*Volunteer*
03/15/2011	Tour guide for prospective National Merit Scholar at OU
04/3/2010	High School Girl's Day Sponsored by SWE-*Volunteer*
04/1/2010	Tour guide for prospective honors student to come to OU
April 2010	Big Event Day of Community Service at OU-*Group Leader*
11/21/2010	Sooner Saturday at OU-*Volunteer*
02/09/2010	Women in Science Conference/Engineering Fair at OU-*Volunteer*
Fall 2010	Member of HKN leadership team that successfully brought the national conference to the University of Oklahoma
April 2009	Big Event Day of Community Service at OU-*Volunteer*

CONFERENCES/SYMPOSIUMS

September 2020	2020 Carnegie Mellon Forum on Biomedical Engineering and Annual Symposium of International Academy of Medical and Biological Engineering-*Poster*
July 2020	42nd Annual International Conference of the IEEE Engineering in Medicine and Biology Society (EMBC) -*Talk*
April 2019	2nd Annual Women in STEM Symposium, Johns Hopkins-*Planning Committee*
February 2019	Association for Research in Otolaryngology (ARO) Conference
April 2019	Women in STEM Symposium, Johns Hopkins-*Volunteer*
January 2018	North American Neuromodulation Society (NANS) Conference-*Poster*
January 2018	Association of Faculties for the Advancement of Community College (AFACCT) Conference- *Talk*
March 2013	Workshop on Control of Cyber-Physical Systems, Johns Hopkins
Summer 2011	Phi Sigma Pi National Conference
Spring 2010	Eta Kappa Nu National Conference, University of Oklahoma-*Leadership Team*